

FORMATION OF TIDAL CAPTURES AND GRAVITATIONAL WAVE INSPIRALS IN BINARY-SINGLE INTERACTIONS

JOHAN SAMSING^{1,*}, MORGAN MACLEOD^{2,*}, ENRICO RAMIREZ-RUIZ³

Draft version October 10, 2018

ABSTRACT

We perform the first systematic study on how dynamical stellar tides and general relativistic (GR) effects affect the dynamics and outcomes of binary-single interactions. For this, we have constructed an N-body code that includes tides in the affine approximation, where stars are modeled as self-similar ellipsoidal polytropes, and GR corrections using the commonly-used post-Newtonian formalism. Using this numerical formalism, we are able to resolve the leading effect from tides and GR across several orders of magnitude in both stellar radius and initial target binary separation. We find that the main effect from tides is the formation of two-body tidal captures that form during the chaotic and resonant evolution of the triple system. The two stars undergoing the capture spiral in and merge. The inclusion of tides can thus lead to an increase in the stellar coalescence rate. We also develop an analytical framework for calculating the cross section of tidal inspirals between any pair of objects with similar mass. From our analytical and numerical estimates we find that the rate of tidal inspirals relative to collisions increases as the initial semi-major axis of the target binary increases and the radius of the interacting tidal objects decreases. The largest effect is therefore found for triple systems hosting white dwarfs and neutron stars. In this case, we find the rate of highly eccentric white dwarf - neutron star mergers to likely be dominated by tidal inspirals. While tidal inspirals occur rarely, we note that they can give rise to a plethora of thermonuclear transients such as Ca-rich transients.

1. INTRODUCTION

Stars in dense stellar systems evolve very differently than those in the solar neighborhood. In an environment of extreme stellar density, like a globular cluster (GC), close encounters between stars are frequent (Heggie 1975; Hut & Bahcall 1983; Hut 1983; Hut et al. 1992; Hut 1993; Heggie & Hut 1993). Binary-single dynamical encounters, which occur when a single star passes close to a binary and perturbs it, are particularly likely. These encounters are much more frequent than single-single stellar encounters because the orbit of the binary acts as a net – sweeping passing single stars into periods of resonant triple-object interactivity which are characterized by the formation and dissolution of temporary binary pairings. As such, binary-single interactions are responsible for shaping the populations of close binaries in dense clusters (Heggie 1975; McMillan 1991; Hut et al. 1992; Baumgardt et al. 2002; Ivanova et al. 2005b,a; Fregeau et al. 2009; Verbunt & Freire 2014).

Because the energy and momentum are randomized during these chaotic triple interactions, very close passages between pairs of objects are possible (e.g., Hut & Inagaki 1985; McMillan 1986; Valtonen & Karttunen 2006). During close passages deviations in the dynamics from the behavior of point masses in the limit of Newtonian gravity can become apparent. Samsing et al. (2014) studied the modification of binary-single dynamics by the inclusion of gravitational wave (GW) energy losses. This work showed a counterintuitive result: passages close enough to modify the dynamics are actually most common in systems involving *wide* target binaries. We typically associate general relativistic corrections with being most important in compact systems, but Samsing et al.

(2014) show that the likelihood of generating a very close encounter actually rises as the target binary widens because its larger cross section sweeps in the most perturbing stars.

This paper focuses on stellar tides, another commonly neglected physical ingredient in the full N -body equation of motion of stars. Stellar tides can be excited in close passages and much like gravitational radiation, the amplitude of tidally-excited oscillations is very sensitive to the passage distance between two objects. Tides play a role in stellar dynamics when stars are sufficiently close that there is an appreciable difference in gravitational force across the object radius. The relative tidal force scales to leading order as $(R/r)^3$ for a perturber at distance r from a star with radius R . The associated energy transfer has a much steeper dependence on r (Press & Teukolsky 1977, which we refer as PT for the rest of the paper). Thus tides can become important when objects come within a few stellar radii of each other.

Previous work on how dynamical tides might affect GC evolution has mostly been related to the role of binaries that are formed through two-body tidal captures (Fabian et al. 1975; Press & Teukolsky 1977; Lee & Ostriker 1986; McMillan et al. 1987). These "two-body" binaries have been suggested to, for example, help reverse the contraction of GC core collapse long before binaries formed by pure "three-body" interactions are created (Krolik 1983; Ostriker 1985; McMillan 1986). Tidally formed binaries also have potentially observable consequences and were initially suggested to explain GC X-ray sources (Fabian et al. 1975; Clark 1975). Numerical modeling and observations have shown that few-body interactions must play a role not only in the formation and disruption of X-ray binaries (Hut & Verbunt 1983; Pooley et al. 2003; Pooley & Hut 2006; Ivanova et al. 2010; Ivanova 2013; Verbunt & Freire 2014), but of all compact binaries in dense stellar systems (e.g., Sigurdsson & Phinney 1993, 1995; Ivanova et al. 2006, 2008). This further includes compact neutron star binaries which are believed to be the progenitors of short gamma-ray bursts (SGRBs; Grindlay et al. 2006; Lee et al. 2010). Other distinct features of dynamically formed

¹ Department of Astrophysical Sciences, Princeton University, Peyton Hall, 4 Ivy Lane, Princeton, NJ 08544, USA

² School of Natural Sciences, Institute for Advanced Study, 1 Einstein Drive, Princeton, New Jersey 08540, USA

³ Department of Astronomy and Astrophysics, University of California, Santa Cruz, CA 95064, USA

* Einstein Fellow

binaries include high eccentricity at merger, which can give rise to a rich variety of electromagnetic and GW signatures for black holes and neutron stars (Stephens et al. 2011; East et al. 2012; Gold et al. 2012; East & Pretorius 2012; East et al. 2013; Samsing et al. 2014).

The role of dynamical encounters has been further linked to the observed distribution of pulsars (Camilo & Rasio 2005; Freire 2013; Verbunt & Freire 2014). In particular, the observed population of single millisecond-pulsars (MSPs) in GCs suggests that few-body interactions must happen frequently with outcomes that both assemble and disrupt compact binaries (Freire 2013; Verbunt & Freire 2014). Few-body interactions involving two or more stars are also likely to result in stellar mergers (Fregeau et al. 2004). The remnants of such mergers have been proposed to partially explain the observed population of so-called blue stragglers (BSs; Sandage 1953). However, the leading formation mechanism of BSs is still under debate (e.g., Leigh et al. 2011, 2013; Knigge 2015), with formation mechanisms ranging from isolated mass transfer (Geller & Mathieu 2011) to secular dynamics (Perets & Fabrycky 2009) and resonant few-body interactions (Fregeau et al. 2004).

Despite the clear importance of few-body interactions in shaping the distributions of binaries and singles, no systematic study has been done of how tidal effects might affect the outcomes. The nature of tidal encounters also remains uncertain. In fact, simulations and semi-analytical models indicate that a tidally formed binary may lead to a merger rather than a stable binary (Kochanek 1992; Rasio 1993), a concern that was also raised in the original paper by Fabian et al. (1975). The evolution of the tidal capture itself has been studied using different analytical prescriptions: Mardling (1995a,b) showed using a linear mode analysis that if one takes into account the evolving oscillatory state of the stars on the orbital evolution, tidal captures are likely to undergo quasiperiodic or even random walk behavior. Similar behavior has also been discussed and seen in work related to the non-linear affine model developed by Carter & Luminet (1985) and Luminet & Carter (1986), further studied by e.g. Kochanek (1992), Lai et al. (1993b, 1994a,b,c) and Lai & Shapiro (1995), and later generalized by Ivanov & Novikov (2001) and Ivanov et al. (2003). Non-linear mode couplings could therefore play a role in the problem of a tidal encounter since the mode excitation spectrum of the star determines the dynamical evolution at subsequent passages. The outcome is therefore intimately linked to the problem of how the energy is dissipated during the evolution, which remains an open question (e.g., Ogilvie 2014).

GC simulations including approximations of tidal effects have been performed (Mardling & Aarseth 2001), but to our knowledge, there is little systematic study of how dynamical tides play a role in few-body systems. Earlier works, particularly by Hut & Inagaki (1985) and McMillan (1986), have discussed the effect of tides and finite sizes. However, their results are based on point-particle simulations and the few-body systems they study are not evolved consistently with tides. Recent studies by, e.g., Gaburov et al. (2010) have modeled a few binary-single interactions using smoothed particle hydrodynamics (SPH). However, their limited sample mainly consists of very hard target binaries due to the heavy computational cost of SPH simulations, and are therefore not representative for the wide distribution of binary-single interactions that are known to occur in dense stellar systems.

The first clear insight about how tides might affect binary-single interactions in general, was given by Kochanek (1992),

who correctly suggested that tidal effects in three-body interactions will lead to two-body tidal captures during the chaotic evolution of the triple system. Furthermore, Kochanek (1992) imagined that these tidally formed binaries probably have an orbital distribution different from those formed by two-body captures in the field.

In our work we study close three-body encounters using an N -body prescription where the orbital dynamics is evolved consistently with both tides and GR. We show that the main effect of including tides is the formation of two-body tidal captures during the three-body evolution, in agreement with earlier predictions by Kochanek (1992). Using both numerical and analytical arguments we illustrate that the relative rate of these tidal captures increases as the radius of the tidal object decreases relative to the size of the initial target binary. In the astrophysical context, tides therefore show the largest effect when the perturbed object is a white dwarf.

Our analysis of the role of tides in binary-single dynamics proceeds as follows. We discuss the general properties of binary-single encounters and build some intuition for the possible role of tides in shaping these encounters in Section 2. In Section 3 we describe a numerical formalism for including tidal excitation in N -body encounters by treating stars as compressible ellipsoids. In Section 4 we describe results of scattering experiments of large numbers of binary-single encounters. In Section 5 we derive analytical relationships to interpret the dependence of these results on stellar type and binary properties. Finally, in Section 6 we discussed our findings while our conclusions are presented in Section 7.

2. BINARY-SINGLE INTERACTIONS AND TIDAL EFFECTS

We begin our exploration of tidal effects in binary-single stellar interactions by reviewing some of the basic properties of these encounters in the point-mass limit approximation. We then consider the possible role of finite-size objects in shaping the nature of the interactions and the range of possible outcomes.

2.1. Binary-Single Interactions

A binary in a dense stellar environment is subject to weak and strong perturbations from the surrounding stars. In a typical dense stellar system, many of these perturbing stars will be single stars (Heggie 1975; Hut et al. 1992). The resulting binary-single stellar encounters happen at a rate which depends on the semimajor axis (SMA) of the binary, a_0 , the total mass of the three interacting objects, m_{tot} , and the relative velocity of the perturbers at infinity, v_∞ (the velocity dispersion of the stellar system). A larger SMA makes the binary a larger target for interloping objects, and a larger total mass enhances gravitational focusing towards the binary.

In this paper, we focus on close binary-single encounters: those in which the single object reaches a pericenter distance – with respect to the center of mass (COM) of the binary – of approximately the binary SMA a_0 (Samsing et al. 2014). The cross section has contributions from the geometrical scale of the binary, $\approx \pi a_0^2$, and from gravitational focusing. In the limit when gravitational focusing dominates, the close interaction (CI) cross section can be written as (Samsing et al. 2014),

$$\sigma_{\text{CI}} \approx \frac{2\pi G m_{\text{tot}} a_0}{v_\infty^2}. \quad (1)$$

The corresponding event rate of close interactions experi-

enced by this binary is given by

$$\Gamma_{\text{CI}} \approx n\sigma_{\text{CI}}v_{\infty}, \quad (2)$$

where n is the number density of perturbing stars.

Gravitational focusing is dominant in establishing the binary cross section when the binary is *hard* relative to the surrounding stellar system. Hard binaries are those that are sufficiently compact that the net energy of a typical three body encounter is negative (Hut & Bahcall 1983). This is fulfilled when v_{∞} is less than the characteristic velocity of the binary, v_c , defined as (Hut & Bahcall 1983)

$$v_c^2 \equiv G \frac{m_1 m_2 (m_1 + m_2 + m_3)}{m_3 (m_1 + m_2)} \frac{1}{a_0}, \quad (3)$$

where 1 and 2 refer to the two stars initially in the binary, and 3 to the incoming perturber. In the opposite case, *soft* binaries have net positive energy when the energy of a typical perturber is included. Heggie (1975) has shown that (as a result of their energetics) hard binaries tend to persist and tighten in dense stellar systems, while soft binaries tend to dissolve. The maximum SMA a binary can have without dissolving, denoted a_{HB} , is therefore set by the limit where $v_c \approx v_{\infty}$. In the equal mass case, we see from Equation (3) that $a_{\text{HB}} \propto m/v_{\infty}^2$.

Because the net energy is negative in an encounter involving a hard binary (HB), the triple system formed by the binary and the perturbing single object may pass through many iterations before a final configuration is attained. We call these multipassage encounters *resonant* interactions. They are characterized by the formation and disruption of many intermediate state (IMS) binaries before an eventual outcome (Samsing et al. 2014). In these chaotic interactions, memory of the initial configuration is lost and all objects are therefore equally likely to be ejected (if they are identical).

In general, several possible outcomes result from a binary-single close interaction. In the limit of Newtonian point masses, these include:

- *ionization* of the system (all three objects are mutually unbound). This outcome can occur in the soft-binary regime but not in the HB limit.
- a *fly-by* encounter, in which the binary survives the encounter but its original orbit is modified as a result.
- an *exchange* encounter, in which the perturber exchanges into the binary system, ejecting one of the original binary components.

In GR, an additional outcome is possible:

- an *inspiral* between two compact objects through the emission of GW radiation (Samsing et al. 2014).

These inspirals occur when an IMS binary is generated that has very high eccentricity (and thus small pericenter distance) so that GW losses strongly modify the equation of motion. Samsing et al. (2014) found that this configuration arises primarily in resonant interactions involving hard binaries, where many opportunities for close passages occur before the binary-single encounter concludes.

2.2. Finite Size Objects in Binary-Single Interactions: Collisions and Tides

Having outlined the basic properties of binary-single encounters in dense stellar systems, we move on to consider the

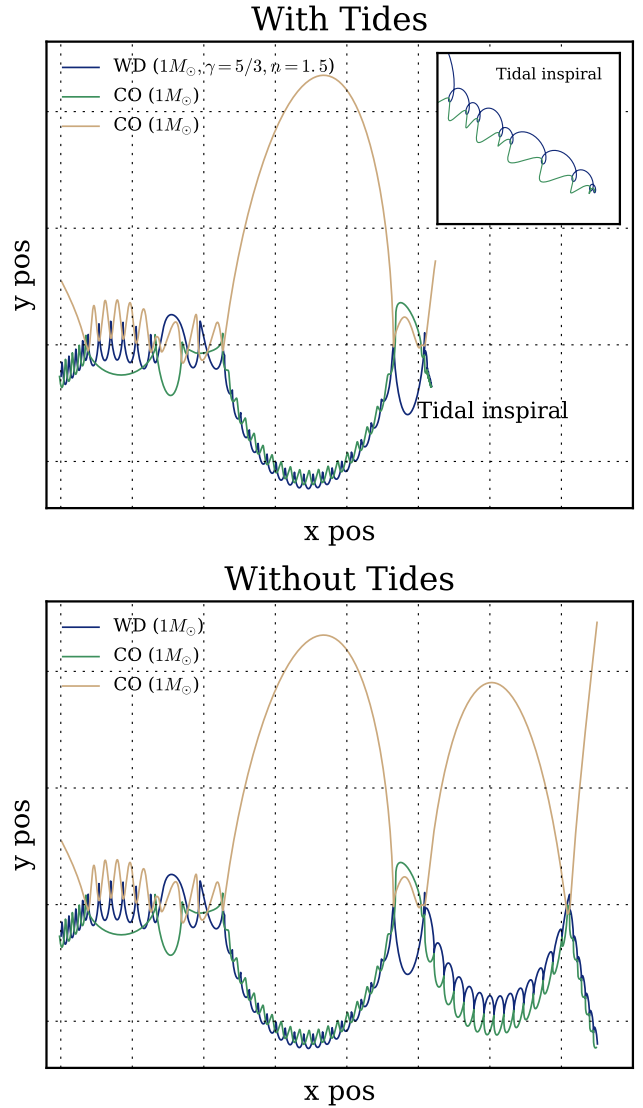


FIG. 1.— Orbital evolution of a binary composed of a white dwarf (WD, blue) and a compact object (CO, green), interacting with a single incoming compact object (CO, brown). The interactions propagate from left to right. The *top plot* shows the evolution if tidal effects are included in the equation of motion, where the *bottom plot* shows the evolution if the WD is modeled as a simple solid sphere. Both simulations have the exact same initial conditions. Each object has a mass of $1M_{\odot}$, the radius of the WD is set to $0.0086R_{\odot}$ and is modeled as a polytrope with adiabatic index $\gamma = 5/3$ and polytropic index $n = 1.5$ (see Section 3). The initial semimajor axis is $5 \cdot 10^{-3}$ AU. As seen in the top plot, when tidal effects are included a close passage between two of the three stars can lead to a tidal capture during the chaotic evolution of the system (indicated by the label *Tidal inspiral*). In this paper we denote such a capture a *tidal inspiral* mainly due its similarity to GW inspirals (Samsing et al. 2014). The insert box at the upper right shows a zoom in on the final few orbits of the inspiral between the WD and the CO. As seen, the orbital evolution is not smooth which is due to the strong coupling between the tidal modes and the orbit. The final stage of the inspiral is a coalescence between the WD and the CO.

structure of the stellar objects involved. If objects have finite size, rather than being point masses, the most obvious new outcome is that two objects may undergo a *collision* if they approach each other with pericenter distance less than the sum of their radii (Hut & Inagaki 1985).

This paper focuses primarily on a second effect: close passages may also excite non-radial oscillations in stars originating from the difference in gravitational force between the

stellar COM and the stellar limb. Tidal forces distort stars during particularly close passages (those with pericenter distance within a few stellar radii for equal mass objects). When a distorted star flies free of this perturbing force, it begins to oscillate (non-radially) around its equilibrium configuration. The quadrupolar fundamental mode is the primary oscillation mode excited with $l = 2$, $m = \pm 2$ in spherical harmonic notation (Press & Teukolsky 1977; Lee & Ostriker 1986; Kochanek 1992). The energy and momentum carried by these oscillations comes at the expense of the orbital motion of the stars. Thus, exciting tidal oscillations drains energy and angular momentum from the orbit of a pair of objects and – by depositing that energy and momentum elsewhere – tidal oscillations can act as a sink term.

By modifying the equation of motion, the inclusion of tides in binary-single encounters has many potential effects on the dynamics and distribution of outcomes. One particularly dramatic outcome is the possibility for a new interaction channel. In some encounters, IMS binaries form which could spiral in from an initially wide orbit toward merger, by transferring orbital energy into tidal oscillations. These tidal capture events, or *tidal inspirals*, as we will refer to them, occur in cases where an IMS binary has high eccentricity and undergoes a very close pericenter passage, leading to strong tidal forcing.

Figure 1 shows two binary-single interactions, each with the same initial conditions. The simulation shown on the *top panel* includes tides, while the simulation shown on the *bottom panel* does not (we use a numerical methodology in integrating these encounters which will be discussed in Section 3). In this particular example we clearly see that a tidal inspiral has formed when tides are included. The formation of an eccentric IMS binary leads to a close, strong tidal interaction. In this way, tidal inspirals are similar to GW inspirals, which also form in rare, very close pericenter passages during resonant interactions. This similarity will be exploited in Section 5, in order to derive a simple yet generalized analytical understanding of such encounters.

Our study focuses on understanding the formation rate of these tidal inspirals, and classifying their effects on the triple dynamics of binary-single encounters. In the subsection below we present some of the characteristic scalings involved in the problem, which can lead to a simple understanding of what combinations of orbital and object parameters can successfully generate tidal inspirals.

2.3. Tidal Captures from Simple Scaling Relations

Here we derive a few fundamental scaling relations in order to illustrate and build intuition for when tides are expected to play a leading role in binary-single interactions. A naive guess is that tides are expected to play a role when the SMA of the target binary, a_0 , is relatively small compared to the radius of the stars, R . However, in the following we show that the dependence is indeed the opposite: tidal outcomes are maximized when a_0 is large compared to R .

For tidal perturbations to alter the evolution of a chaotic binary-single interaction, the energy deposited into tidal oscillations during a close passage between two of the three stars, ΔE_{tid} , must be similar to the total orbital energy of the system, E_0 . Assuming the tidal energy transfer falls off as a simple power-law with pericenter distance, r_p , and that the orbital energy is dominated by the target binary (HB limit), the

energy terms can be written as

$$\Delta E_{\text{tid}} \propto \frac{m^2}{R} \left(\frac{R}{r_p} \right)^\beta \quad \text{and} \quad E_0 \propto \frac{m^2}{a_0}, \quad (4)$$

where $\beta \gtrsim 6$ as we'll discuss later. By equating ΔE_{tid} and E_0 , we can now solve for the pericenter distance at which two stars must pass for tides to have a substantial energetic effect on the triple system. We call this distance r_{tid} , and it scales as

$$r_{\text{tid}} \propto R \left(\frac{a_0}{R} \right)^{1/\beta} \propto R \left(\frac{E_{\text{star}}}{E_0} \right)^{1/\beta}, \quad (5)$$

where $E_{\text{star}} \propto m^2/R$ is the binding energy of the star. The tidal pericenter distance r_{tid} is not merely a constant times R , as has been assumed in many previous studies (e.g. Fregeau et al. 2004): r_{tid} depends on the total energy of the system, E_0 . In particular, r_{tid} increases with a_0 in contrast to R . As a result, the fraction of tidal encounters ($r_p < r_{\text{tid}}$) also increases relative to the fraction of collisions ($r_p < R$). This leaves open the possibility of tidal encounters dominating over collisions. Finally, we note that our scalings for r_{tid} are similar to the well known scalings for the single-single tidal capture radius (Fabian et al. 1975), but with E_0 replaced by $E_\infty \propto mv_\infty^2$, where v_∞ is the velocity dispersion of the stellar system.

Motivated by the scalings in Equation (5), we explore the effect of tides as a function of orbital properties and object compactness. We do this by first using full numerical simulations which include both tidal and GR correction terms. We describe our approach and results in Sections 3 and 4, respectively. This is then followed by an analytical derivation in Section 5 aimed at understanding how tidal and GW captures are formed as a function of target binary separation and object compactness.

3. NUMERICAL METHODS: N -BODY WITH TIDES AND GENERAL RELATIVISTIC CORRECTIONS

For this study we constructed a new N -body code which includes GR effects and dynamical tides. The GR corrections are modeled using the *post-Newtonian* (PN) expansion formalism (Blanchet 2006), while tides are dynamically evolved using the *affine model* of compressible ellipsoidal stars, which allows for the implementation of non-linear stellar deformations (Carter & Luminet 1985). To evolve this system we make use of the ODEPACK, LAPACK and GSL libraries. N -body codes including tides at the linear PT level are available (Mardling & Aarseth 2001), however, it is essential to our study to have a fully dynamical model since our interactions often undergo several strong, and sometimes simultaneous, encounters between two or more objects. The affine model also performs better than the PT model during very close passages, which is important since these are associated with the largest transfer of energy and angular momentum between the tides and the binary's orbit.

We numerically estimate outcome cross sections using a standard Monte Carlo (MC) approach (Hut & Bahcall 1983), which in our case, makes use of an MPI parallelized version. In the following sections we describe in further detail our GR and tidal implementations in the N -body code. Regarding notation, we use boldface below for denoting vectors and matrices.

3.1. General Relativistic Corrections

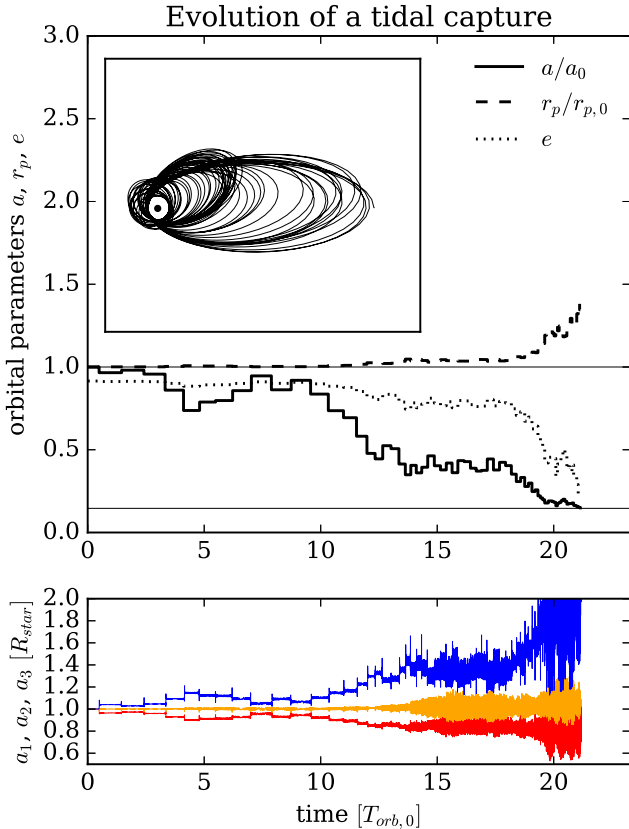


FIG. 2.— Evolution of a strong tidal capture with initial pericenter $r_p \sim 2R_\odot$ and semimajor axis 0.1AU , between a neutron star ($1.4M_\odot$) and a solar type star ($1M_\odot$, $1R_\odot$, $\gamma = 5/3$, $n = 3$). The simulation is performed with our new N -body code which includes tidal effects using the affine model (Carter & Luminet 1985). This model allows for non-linear ellipsoidal stellar deformations, which are consistently evolved and coupled to the orbital evolution of the N -body system. *Top*: Evolution of semimajor axis a , pericenter r_p , and corresponding eccentricity e , as a function of time for the evolving binary. The change in the parameters results from the orbit sinking energy and angular momentum into the tidal modes. As can be seen, the orbital parameters are performing a quasi-random walk due to the short time scale of the tidal oscillations relative to the binary’s orbital time. The *upper left* panel shows the trajectory of the neutron star relative to the star. *Bottom*: Corresponding time evolution of the three principal axis of the ellipsoidal model of the star. The star is quite distorted at the end of the encounter and the outcome is therefore likely to be a partial disruption.

We model the effects from GR, such as GW radiation, using the PN formalism (Blanchet 2006). In this formalism GR is included by simply adding correction terms of order v/c to the classical Newtonian acceleration $\propto 1/r^2$. Following this framework, the acceleration of an object with mass m_1 due to an object with mass m_2 can be written as

$$\mathbf{a} = \mathbf{a}_0 + c^{-2}\mathbf{a}_2 + c^{-4}\mathbf{a}_4 + c^{-5}\mathbf{a}_5 + \mathcal{O}(c^{-6}), \quad (6)$$

where the standard Newtonian acceleration, \mathbf{a}_0 , is given by

$$\mathbf{a}_0 = -\frac{Gm_2}{r_{12}^2} \hat{\mathbf{r}}_{12}. \quad (7)$$

Here we have defined the separation vector $\mathbf{r}_{12} = \mathbf{r}_1 - \mathbf{r}_2$, where its magnitude is $r_{12} = |\mathbf{r}_{12}|$ and its direction is $\hat{\mathbf{r}}_{12} = \mathbf{r}_{12}/r_{12}$. The terms, \mathbf{a}_2 and \mathbf{a}_4 , conserve energy and account for the periastron shift. These terms play a key role when describing hierarchical secularly evolving systems (e.g. Naoz et al. 2013). The leading order term that represents the energy and momentum loss carried away by GW radiation is \mathbf{a}_5 , often de-

noted the 2.5PN term. For our study, the 2.5PN correction is the only relevant term to include since any effects from the lower order precession terms will simply average out when calculating the cross section from a large number of scatterings (Gültekin et al. 2006; Samsing et al. 2014). The 2.5PN term takes the following form

$$\mathbf{a}_5 = \frac{4}{5} \frac{G^2 m_1 m_2}{r_{12}^3} \left[\left(\frac{2Gm_1}{r_{12}} - \frac{8Gm_2}{r_{12}} - v_{12}^2 \right) \mathbf{v}_{12} + (\hat{\mathbf{r}}_{12} \cdot \mathbf{v}_{12}) \left(\frac{52Gm_2}{3r_{12}} - \frac{6Gm_1}{r_{12}} + 3v_{12}^2 \right) \hat{\mathbf{r}}_{12} \right], \quad (8)$$

where the relative velocity scalar, v_{12} , and vector, \mathbf{v}_{12} , are defined following the same conventions as in Blanchet (2006). Further details can be found in Samsing et al. (2014), where we have shown that the main effect from this correction is the formation of binaries that inspiral due to GW emission during the resonant interaction.

3.2. Tidal Corrections

We dynamically evolve stellar tides using the affine model developed in Carter & Luminet (1985). In this model, the tidal response and the coupling to the orbit is calculated assuming the star can be described by a triaxial object composed of self-similar ellipsoids. The model accounts for different radial density and pressure profiles for the distorted star. As a result, one can self-consistently evolve close encounters between stars with different polytropic index, mass and radius. The advantage of the model is that it accounts for the non-linear deformations of the star along its triaxial axes, while its disadvantage is that it only accounts for the evolution of the $l = 2$ mode. However, as pointed out by, for example, Kochanek (1992), the $l = 2$ f -mode is expected to dominate the energy transfer. This makes the affine model a great choice for evolving highly dynamically N -body systems. Work by Lai et al. (1994a) has also compared its validity to full SPH simulations. More complicated versions of the model, which incorporate mass loss and allow for the principle axis to evolve independently throughout the star have been constructed (Ivanov & Novikov 2001; Ivanov et al. 2003). Yet, the corrections in these models come at a very high computational cost.

In what follows we briefly discuss the basic evolution equations of the affine model, but refer the reader to the extensive literature on the subject for more details (Carter & Luminet 1985; Luminet & Carter 1986; Kochanek 1992; Kosovichev & Novikov 1992; Lai et al. 1993b,c, 1994b,a; Lai & Shapiro 1995; Diener et al. 1995; Ogawaguchi & Kojima 1996; Ivanov & Novikov 2001; Ivanov et al. 2003). In order to validate our code formalism, we compared our results against the 2-body encounter outcomes presented in Lai et al. (1994c).

In the affine model the position of a fluid element inside the star at time t is given by

$$x_i(t) = q_{ij}(t) \hat{x}_j, \quad (9)$$

where q_{ij} is a 3×3 matrix, \hat{x}_j is the fluid position at time $t = 0$, and summation over repeated indices is assumed. The tidal evolution of the star is completely determined by the evolution of the components of q_{ij} . The evolution of a star experiencing a deformation \mathbf{q} and its respective coupling to other stars and their mutual orbital motion can found using the Lagrangian formalism. In our case, the Lagrangian of the full N -body system is given by

$$L = L_I + L_E, \quad (10)$$

where L_I is the *internal* Lagrangian which relates to the internal energy of the individual stars, and L_E is the *external* Lagrangian which is composed of the kinetic COM energy and the potential energy between the interacting stars. The internal Lagrangian is given by

$$L_I = T - U - \Omega \quad (11)$$

where T is the stellar kinetic energy, U is the gas energy, and Ω is the self-gravitational potential energy. Each of these energy terms take the following form for a single star in the affine model,

$$T = \text{Tr}[T_{ij}], \quad T_{ij} = \frac{1}{2} \dot{q}_{ia} \dot{q}_{ja} \mathcal{M}_* \quad (12)$$

$$U = -\frac{\Omega_*}{3(\gamma-1)} |\mathbf{q}|^{1-\gamma} \quad (13)$$

$$\Omega = \text{Tr}[\Omega_{ij}], \quad \Omega_{ij} = \frac{1}{2} \Omega_* |\mathbf{S}|^{-1/2} \mathbf{A} \mathbf{S} \quad (14)$$

where $\text{Tr}[Y_{ij}]$ denotes the trace of matrix Y_{ij} , $|\mathbf{Y}|$ denotes the determinant of \mathbf{Y} , \dot{q} is the time derivative of q , $\mathbf{S} = \mathbf{q}\mathbf{q}^T$ where \mathbf{T} is here the transpose, \mathcal{M}_* is the scalar quadrupole moment of the spherical star⁵, γ is the adiabatic index of the stellar fluid, and

$$\Omega_* = -\frac{3}{5-n} \frac{Gm^2}{R}, \quad \text{and} \quad (15)$$

$$\mathbf{A} = |\mathbf{S}|^{1/2} \int_0^\infty du \frac{(\mathbf{S} + u\mathbf{I})^{-1}}{|\mathbf{S} + u\mathbf{I}|^{1/2}}. \quad (16)$$

Here the matrix \mathbf{I} is the identity matrix, u denotes an integration variable, m and R denotes the mass and the radius of the star, respectively, and n the stellar polytropic index. The elliptical integral needed for calculating \mathbf{A} has to be performed at each time step⁶. The external Lagrangian is given by

$$L_E = K - \Phi, \quad (17)$$

where K is the COM kinetic energy and Φ is the total potential energy of the system. The term Φ is in the case of two stars, 1 and 2, found by integrating the potential of star 1 over the density distribution of star 2 and viceversa. To quadrupole order this term takes the form,

$$\Phi_{12} = -\frac{m_1 m_2}{|X|} - \frac{1}{2} C_{ij} \left[m_1 \mathcal{M}_*^{(2)} S_{ij}^{(2)} + m_2 \mathcal{M}_*^{(1)} S_{ij}^{(1)} \right] \quad (18)$$

where C_{ij} is the tidal tensor here defined as

$$C_{ij} = \frac{3X_i X_j - |X|^2 I_{ij}}{|X|^5}, \quad (19)$$

and \mathbf{X} is the relative position vector between the two stars. The final L_E is given by the sum of the individual kinetic terms and the pairwise potential terms. From applying the Lagrange formalism, the equation of motion (EOM) of the deformation matrix \mathbf{q} for a single star is given by

$$\ddot{q}_{ia} = q_{aj}^{-1} (\Omega_{ij} - |\mathbf{q}|^{1-\gamma} \Omega_* I_{ij} / 3) / \mathcal{M}_* + \sum_n m_n C_{ij}^{(n)} q_{ja}, \quad (20)$$

⁵ A table with calculated values for stars with different polytropic index n is given by Diener et al. (1995) in Table A1.

⁶ A significant improvement in speed can be achieved by solving the integral in coordinates where \mathbf{S} is diagonal, in this case the integral reduces to the Carlson's incomplete integral of the third kind (Kochanek 1992).

where the COM acceleration term arising from tidal couplings, here denoted \mathbf{a}_{TC} , is found to be

$$\mathbf{a}_{\text{TC}} = \frac{1}{2m} \sum_n Q_{ijk}^{(n)} \left(m \mathcal{M}_*^{(n)} S_{ij}^{(n)} + m_n \mathcal{M}_* S_{ij} \right). \quad (21)$$

The tensor Q_{ijk} is here the derivative of the tidal tensor C_{ij} with respect to the relative COM coordinate X_k , which we find takes the following form,

$$Q_{ijk} = \frac{3X_k}{|X|^5} \left[\frac{\partial X_i X_j}{\partial X_k} \frac{1}{X_k} - 5 \frac{X_i X_j}{|X|^2} + I_{ij} \right]. \quad (22)$$

For the sums over index n in the equations above, one has to sum over all stars or objects in the N -body system except for the star in question.

We do not include tidal energy and angular momentum dissipation within oscillating stars for the results presented in this paper – tidally induced stellar oscillations are as a result not damped, and can therefore exchange energy and angular momentum with the COM orbital motion throughout the full interaction. This can result in long term chaotic behavior (See Figure 2).

The non-dissipative assumption formally corresponds to the limit where the characteristic orbital time is less than the dissipation time (see Section 3 in Novikov et al. 1992, for a discussion on how a tidal capture undergoing multiple passages depends on the relative values for the viscous, orbital and Kelvin-Helmholtz time-scales). The main reason for making this assumption, is simply that the non-linear tidal dissipation is still very poorly understood. It is nonetheless possible to include an estimate for the dissipation in the affine model by introducing a shear viscosity term (Lai et al. 1994c). However, it is highly uncertain how and where the heat deposition occurs within the perturbed star. One consequence of dissipation is expansion followed by mass loss of the star, which could lead to a tidal runaway. As a result, one would expect more tidal inspirals to form in our simulations if dissipation is swift. The results we report here thus serve as strict lower limit to the tidal inspiral rate and should be considered as such. Several studies have been done on damping and dissipation (McMillan et al. 1987; Kochanek 1992; Kumar & Goodman 1996; Ogilvie 2014), and we are currently working on prescriptions for including both dissipation and mass loss into the affine model⁷.

For our analytical estimation of the tidal inspiral cross section, which is presented in Section 5, we assume that the orbital energy loss during each pericenter is constant. This corresponds to the limit where the tidal energy is fully radiated away from the system between each subsequent passages. The overall agreement between this analytical model and our simulations, shown in Figure 4, indicates that dissipation will probably not change the relative scalings of the inspiral cross section and it is likely that only the normalization will be affected. We expect that our upcoming work will shed light on this matter.

3.2.1. Tidal Capture Example

An example of a tidal capture between a neutron star and a solar type star is shown in Figure 2. The chaotic evolution of

⁷ Mass loss is possible in the extended model presented in Ivanov & Novikov (2001) and Ivanov et al. (2003). For an implementation of linear tides in N -body codes we refer the reader to Mardling & Aarseth (2001).

the SMA (solid black line) is due to the tidal mode-orbit coupling that is consistently modeled in the affine model. Since we don't include dissipation, the two stars are not able to merge and are unable to come closer than their initial pericenter distance r_p . Angular momentum is stored in the tidal modes and in the affine model, this scales with the corresponding change in energy ΔE by (Kochanek 1992),

$$\Delta L \approx \Delta E \sqrt{15 M_* / |\Omega_*|}. \quad (23)$$

However, this change is very small compared to the initial orbital angular momentum L_0 . If we for example consider a tidal capture from an orbit with $a_0 > r_p$, one can easily see that the change ΔL relative to L_0 is small and it is given by $\Delta L/L_0 \propto (R/a_0)$. The analytical solution to the stellar separation at circularization ($e = 0$) when including the ΔL correction term is shown by the lower horizontal solid black line in the upper plot in Figure 2 (slightly lower than $2r_p$).

We find that for some strong tidal captures the two stars merged once their orbit is circularized. This is due to the tidal acceleration term \mathbf{a}_{TC} , which for small binary separation becomes steeper than the point mass potential and causes the instability (similar to the innermost stable orbit in GR, Lai & Shapiro 1995). While we easily identified when this happens, understanding the outcome of such strong tidal interactions requires the use of full hydro simulations. For this reason, in our N -body experiments we keep track of binaries that circularize (tidal inspirals) and not only binaries that merge due to this instability. The dynamical instability of close binaries in the affine limit was extensively explored by Kochanek (1992) and Lai et al. (1994a).

3.2.2. Monte Carlo Estimation of Cross Sections

We follow standard prescriptions for calculating scattering cross sections for a given outcome type O_i by performing N_{tot} binary-single interactions with isotropic sampling across a disc at infinity with radius b (see e.g., Hut & Bahcall 1983; Samsing et al. 2014). The corresponding cross section for outcome O_i can be estimated by

$$\sigma_i = \frac{N_i}{N_{\text{tot}}} \pi b^2, \quad (24)$$

where the total number of outcomes of type O_i from that scattering set is denoted by N_i . The corresponding error is given by

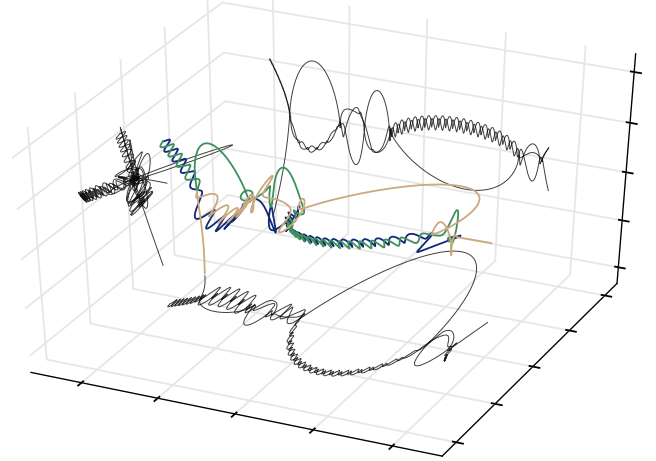
$$\Delta \sigma_i = \frac{\sqrt{N_i}}{N_{\text{tot}}} \pi b^2. \quad (25)$$

The set of interactions that did not lead to an outcome within the time limits were subsequently assumed to have the same final outcome distribution as the set of resonant interactions. We do not include this correction when estimating outcome errors.

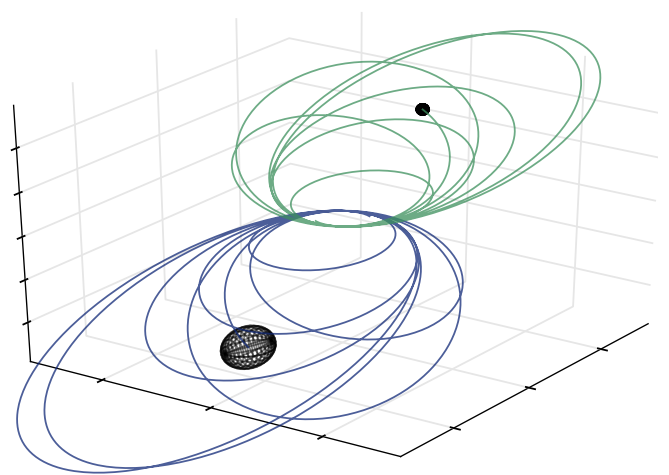
3.2.3. Definition and Identification of Endstates

A state is identified as an *exchange* if the three-body system evolves into a binary and an unbound single where the single was initially part of the target binary (the initial perturber has exchanged into the target binary). We use a binary-single tidal threshold of 0.01 to decide if a triple state can be labeled a binary-single state (see, e.g., Fregeau et al. 2004). We do not distinguish between exchanges arising from direct interactions (DI) and resonant interactions (RI), respectively (for

Binary-Single Interaction (Full)



Final Tidal Interaction (Zoom in)



Dynamical evolution of final inspiral

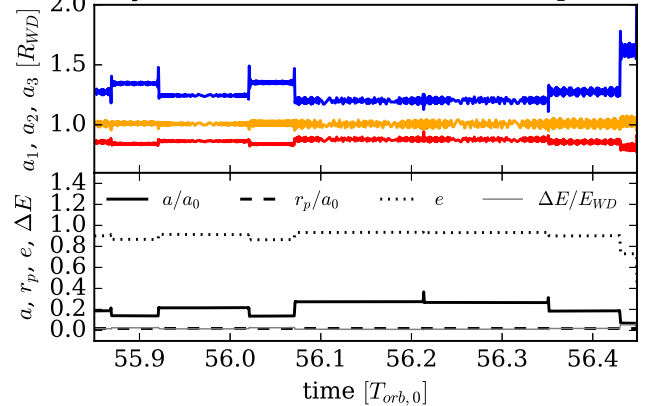


FIG. 3.— Formation of a tidal inspiral between a white dwarf (WD) and a compact object (CO) during a resonant interaction resulting from an initial binary-single interaction. The example is the same as the one shown in the top plot of Figure 1. *Top*: Illustration of the binary-single interaction propagating from left to right. The colored lines show the evolution of the objects with the blue line representing the WD. Projections of the interaction are shown with thin black lines. *Center*: Zoom in on the final few orbits of the tidal inspiral between the WD (extended object) and the CO (black dot). The ellipsoidal shape the WD has acquired during the inspiral is here clearly seen. *Bottom*: Time evolution of the three principle axis of the WD as the WD and the CO spiral in (top window) and corresponding orbital parameters including the energy deposited into the WD, ΔE , in units of $E_{WD} \equiv m_{WD}^2/R_{WD}$ (bottom window). The time range matches the orbits shown in the center plot. Similar inspirals form when using full hydrodynamical prescriptions (Lorén-Aguilar et al. 2010), where the endstate is likely to be a thermonuclear transient (e.g. Rosswog et al. 2009; Raskin et al. 2012).

a definition of DI and RI the reader is refer to [Samsing et al. 2014](#)).

We define a *collision* when two objects with initial unperturbed radii R_1 and R_2 pass each other within a distance $< (R_1 + R_2)$. We use the unperturbed radii even if the stars are being tidally distorted. In this way we can directly compare the collision rates with and without tidal corrections, which provides us with a clear estimate for how the dynamics are altered when tidal excitations are included. This way of defining a collision is normally known as the sticky star approximation, and is the simplest way of including finite size effects ([Fregeau et al. 2004](#)).

An *inspiral* is defined here by a state composed of a binary with a SMA less than some value $a_{\text{insp}} \ll a_0$ and a bound single. We find that setting $a_{\text{insp}} = 6(R_1 + R_2)$ results in a representative sample of inspirals. We are, however, aware that this will miss inspirals forming from pericenter passages $\gtrsim 3(R_1 + R_2)$. The introduction of such a threshold combined with the non-dissipative assumption thus provides us with a strict lower limit on the inspiral cross sections. The difficulties in defining an inspiral is associated to our limited understanding of how a tidal inspiral dissipates energy and transfers angular momentum into the star.

4. NUMERICAL RESULTS

We now estimate exchange, collision, tidal, and GW inspiral cross sections, using the numerical methods described in Section 3. Motivated by the scalings in Section 2.3, we focus on the effect from tides as a function of the initial semimajor axis, a_0 , and the radius of the tidal object, R . We study four different binary-single interactions, two of which have one tidal object (CO-[WD-CO], CO-[MS-CO]) and two where all three objects are identical tidal objects (WD-[WD-WD], MS-[MS-MS]). The brackets indicate what pair is in the initial binary, where CO, WD and MS are short for compact object, white dwarf, and main sequence star, respectively. A CO could here be a black hole (BH) or a neutron star (NS). For these scatterings, we use $\gamma = 4/3$ and $n = 3$ for the WDs, and $\gamma = 5/3$ and $n = 3$ for the MS stars. We limit the computational time for each scattering to 350 initial orbital times due to limited computational resources. Some inspirals will take more time, but those interactions are not possible to follow at the moment. Our complementary analytical estimates, presented in Section 5, therefore serve as a crucial guideline.

To clearly isolate the effect from tides, we only consider cases where all three objects within a given binary-single interaction have the same mass. More physically motivated interactions, including WDs with a realistic mass spectrum, will be explored in upcoming papers.

4.1. Results from our N -body Scatterings

The scattering results from our 3-body experiments are shown in Figure 4. The upper window in each plot shows the cross sections with tides and GR included in the EOM, where the lower window shows the ratio between cross sections calculated with (σ_+) and without (σ_-) tides. The bottom x -axis shows a_0 in AU, while the top shows the compactness a_0/R . The upper limit of $a_0/R \approx 3-4$ is set by computational limitations. The derived cross sections are based on 5×10^4 scatterings per SMA, a_0 . We describe our specific findings below.

4.1.1. CO-[WD-CO]

We first study the binary-single interaction between a CO($1.2M_\odot$) and a [WD($1.2M_\odot$, $0.006R_\odot$)-CO($1.2M_\odot$)] binary. Results are shown in the upper left window in Figure 4. The inclusion of tides clearly results in a population of WD-CO tidal inspirals with a cross section that increases with a_0 . As seen, our analytical estimate (dashed line) from Section 5 indicates that the inspiral rate will exceed the classical collision rate for $a_0 \gtrsim 0.2$ AU. In the bottom window we see that the inclusion of tides doesn't affect either the exchange or collision cross sections in a significant way.

4.1.2. CO-[MS-CO]

The WD from our previous study is now replaced by a MS star ($1.0M_\odot$, $1.0R_\odot$), and the two COs are each given a mass of $1.0M_\odot$. Results are shown in the bottom left window in Figure 4. Tidal inspirals form in this case, but the rate relative to the collision rate is now significantly lower when compared to the HB limit (vertical dotted line). As a result, MS-CO tidal inspirals do not have the necessary range in a_0 to clearly dominate over collisions. From the results in the bottom window, we also in this case conclude that tides do not significantly affect the classical rate of exchanges and collisions.

4.1.3. WD-[WD-WD]

We now consider the interaction between three WDs ($1.2M_\odot$, $0.006R_\odot$). Results are shown in the upper right window in Figure 4. Tidal inspirals form but at a very low rate compared to when one of the objects is a point mass. WD-WD tidal inspirals seem therefore not to contribute significantly to the WD coalescence rate at any a_0 , even at the hard binary limit. More extensive numerical simulations must be performed to investigate this further. Again, we see in the bottom window that the effect from tides does not significantly alter either the exchange or collision cross sections.

4.1.4. MS-[MS-MS]

As a final example, we study the interaction between three MS stars ($1.0M_\odot$, $1.0R_\odot$). Results are shown in the bottom right window in Figure 4. The rate of inspirals relative to collisions is even lower than in the WD-[WD-WD] case, which results in an inspiral rate that is about 1-2 orders of magnitude lower than the collision rate at the hard binary limit. As in the other cases, no strong effects are seen from the inclusion of tides on the exchange and collision cross sections in the lower window.

4.2. Summary of our N -body Scatterings

Our numerical results indicate that tides do not strongly affect the classical exchange and collision cross sections. Instead, when tides are included we see a clear population of tidal inspirals appearing, as initially speculated by [Kochanek \(1992\)](#). For the first time we estimate here the cross section and we find that it increases with a_0 , as opposed to the classical sticky star collision cross section ([Fregeau et al. 2004](#)) which stays nearly flat (the analytical solution also gives a constant cross section). Tidal inspirals therefore have the possibility to dominate over collisions. Because the two stars undergoing the tidal inspiral are likely to merge ([Rasio 1993](#); [Lorén-Aguilar et al. 2010](#)), tidal inspirals can actually dominate the coalescence rate for some interaction channels.

The scattering results further suggest that the rate of tidal inspirals relative to collisions depends on the compactness a_0/R and not only a_0 . For example, if we compare the two datasets

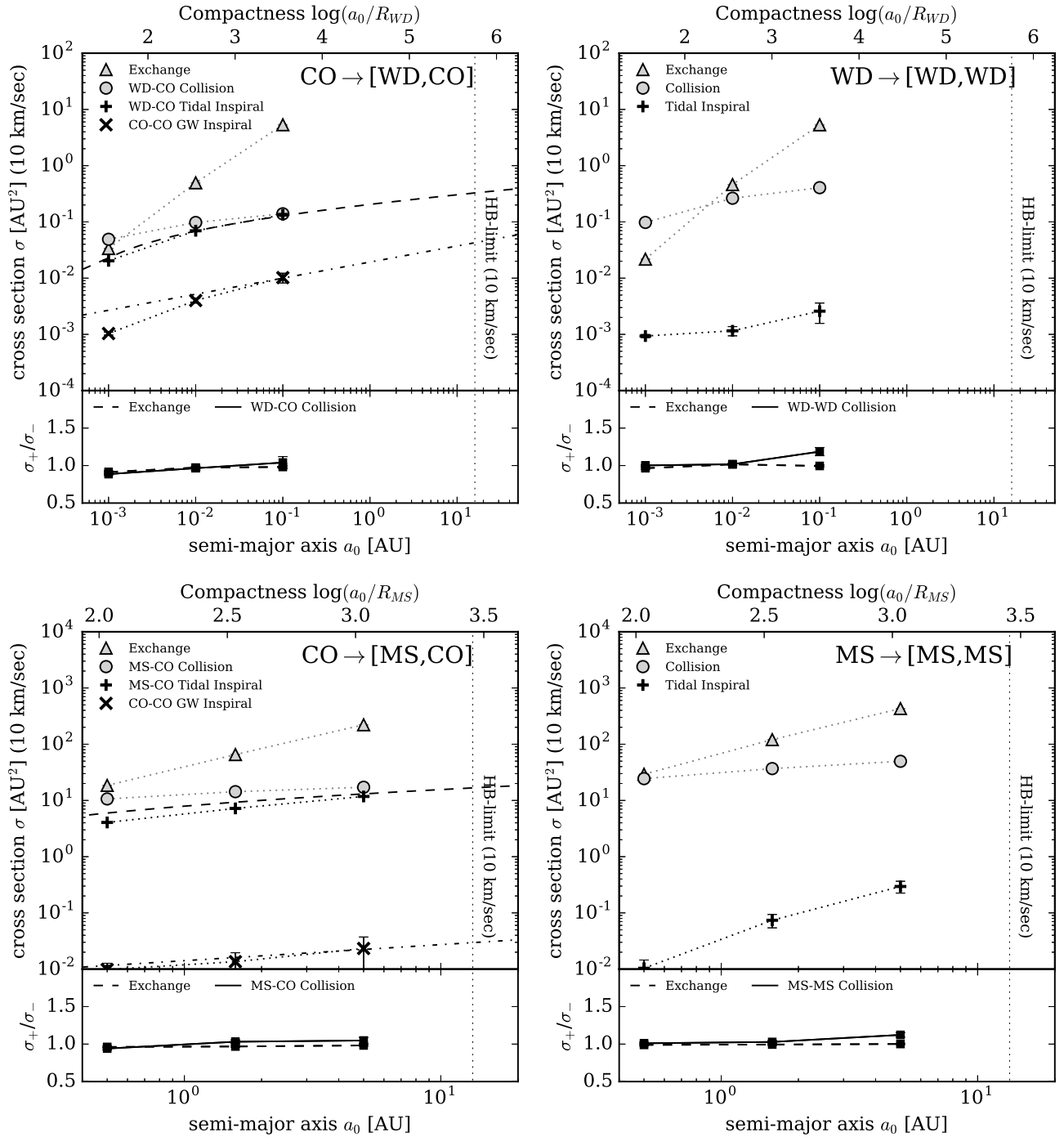


FIG. 4.— Exchange, collision, tidal and GW inspiral cross sections arising from equal mass binary-single interactions, derived using our new N-body code which includes GR and dynamical tides (see Section 3 and 4). The top window in each plot shows the cross sections as a function of the initial SMA, a_0 , of the target binary, where the bottom window shows the ratio between cross sections derived with (σ_+) and without (σ_-) tides included in the EOM. The x-axis at the top of each window shows the SMA scaled by R , where R is the physical radius of the extended tidal object in the triple interaction. As we show in Section 5, the combination a_0/R is the relevant parameter for determining the rate of inspirals relative to collisions. The vertical dotted lines show the HB limit for each system assuming $v_\infty = 10 \text{ km s}^{-1}$: the cross sections are therefore only valid to the left of these lines for this value of v_∞ . The dashed and dashed-dotted lines illustrate our analytical scaling solutions for the tidal and GW inspiral cross sections, respectively, as described in Section 5 and summarized in Figure 6. The scattering results shown here are discussed in Section 4.1.

CO-[WD-CO] and CO-[MS-CO], we see that the inspiral and collision cross sections are equal at the same $\log(a_0/R) \approx 3.5$, but not at a given value of a_0 . This is consistent with the simple scalings from Section 2.3, which depend on a_0/R . The maximum number of inspirals relative to collisions is therefore set by how large a_0/R can be within the HB limit. We know the HB limit scales with the mass of the objects as $a_{\text{HB}} \propto m/v_\infty^2$ with no dependence on R (see Equation 3). As a result, the smaller an object is compared to its mass the larger number of inspirals relative to collisions can be generated during binary-single encounters. This explains why the CO-[WD-CO] channel produces the most inspirals relative to collisions in the scattering examples presented here.

Gravitational wave inspirals between CO-CO binaries are also shown for the WD and MS datasets. The estimated cross sections are fully consistent with the results from Samsing et al. (2014), which provides further credence in our numerical methods. In Samsing et al. (2014) it was shown that these GW inspirals are likely to be the predominating channel for high eccentricity NS-NS GW mergers detectable by LIGO.

Finally, we see that the rate of tidal inspirals between two tidal objects is significantly lower than the rate involving a tidal object and a compact object. There are at least two physical reasons for this. First, an IMS binary with pericenter $R < r_p < 2R$ will lead to a collision instead of an inspiral when both objects are extended. Second, the energy deposited into tides falls off very steeply with distance r (about r^{-9} in the PT model) which here greatly suppresses the formation of inspirals which now need to arise from passages with $r_p > 2R$. Our imposed tidal threshold described in Section 3.2.3 also plays a role; their could very well be inspirals forming through weak interactions evolving over hundred to thousand of orbits that we are not able to follow and identify.

In this work we have considered high mass WDs which have a relative stiff equation of state ($n = 3$), the inspiral cross section could very well be much higher for more realistic low mass WDs which are more prone to tidal deformations due to their lower polytropic index ($n = 1.5$). This motivates our future work on unequal mass interactions and, in particular, those involving WDs and COs.

In the following section we present an analytical model that can explain all the main trends we have seen in our simulations so far. Our numerical scattering results are discussed further in the context of this model in Section 6.

5. ANALYTICAL DESCRIPTION OF INSPIRALS AND COLLISIONS

In this section we present an analytical model for describing the inspiral cross section and how it depends on the properties of the interacting objects and the initial orbital parameters of the binary-single system. In contrast to the simple scalings from Section 2.3, we now correctly account for the energy loss arising from multiple close passages during the binary-single interaction. For all calculations and results we assume the equal mass case, and for tidal inspirals and collisions we further assume the IMS binary is composed of one point-mass perturber and one tidal object with radius R . Further details on the approach we here use to calculate the inspiral cross section can be found in Samsing et al. (2014).

5.1. Energy Losses and Orbital Evolution

We start by considering the orbital energy evolution of an IMS binary with initial eccentricity e , semimajor axis a , and corresponding pericenter $r_p = a(1 - e)$. We assume the binary

loses a constant amount of orbital energy ΔE_p at each pericenter passage due to some effect which only depends on r_p . This is a reasonable approximation for tides and GR, which both have a very steep dependence on r_p (for tides and GR see, e.g., Press & Teukolsky 1977; Blanchet 2006, respectively). The corresponding angular momentum loss ΔL_p is generally small compared to the energy loss (see discussion from Section 3.2.1), r_p and ΔE_p will therefore not change significantly until the binary circularizes. This is also seen in Figure 2. As a result, the orbit averaged energy evolution can be written as,

$$\frac{dE}{dt} \approx \frac{\Delta E_p}{T_{\text{orb}}(t)} \approx \frac{2\Delta E_p}{\pi m^{5/2}} E(t)^{3/2}, \quad (26)$$

where t is time, m is the mass of one of the (equal mass) objects, $T_{\text{orb}}(t)$ is the orbital time of the IMS binary, and $E(t)$ is the corresponding orbital energy. Using this relation, we find the solution for the time evolving SMA $a(t) = m^2/[2E(t)]$ of the IMS binary to be given by,

$$a(t) = a \left(1 - t \frac{\Delta E_p}{\pi \sqrt{2am^3}} \right)^2. \quad (27)$$

We see that the two IMS binary members will merge in a finite time, which corresponds to the limit where $a(t) \rightarrow 0$. This time we define as the inspiral time, t_{insp} , and is from Equation (27) found to be,

$$t_{\text{insp}} = \pi \sqrt{2} \frac{m^{3/2} \sqrt{a}}{\Delta E_p}. \quad (28)$$

For an IMS binary to undergo a successful inspiral, its inspiral time must be less than the time it is isolated from the bound single. Following Samsing et al. (2014), the time that the IMS binary is isolated from the single is given by,

$$t_{\text{iso}} = 2\pi \sqrt{\frac{a_{\text{bs}}^3}{3m}}, \quad (29)$$

where a_{bs} is the semimajor axis of the bound single relative to the IMS binary. This semimajor axis can be found from energy conservation assuming the total orbital energy has not changed before the formation of the IMS binary,

$$E_0 = \frac{m^2}{2a_0} = \frac{m^2}{2a} + \frac{2m^2}{2a_{\text{bs}}}. \quad (30)$$

By solving for a_{bs} in the above equation we find $a_{\text{bs}} = 2a_0/(1 - 1/a')$, where $a' \equiv a/a_0$. Using this expression for a_{bs} , the isolation time t_{iso} from Equation (29) can now be written as

$$t_{\text{iso}} = \frac{4}{\sqrt{3}} \left(\frac{a'}{a' - 1} \right)^{3/2} 2\pi \sqrt{\frac{a_0^3}{2m}}, \quad (31)$$

where the last part equals the orbital time of the initial binary.

While the form of ΔE_p has so far been left general, to proceed we need to specify a functional form for ΔE_p . In the sections below we derive analytical cross sections for an energy loss term of the form $\Delta E_p \propto r_p^{-\beta}$.

5.2. Energy Loss Term of the form $\Delta E \propto r_p^{-\beta}$

We consider the following general form for the orbital energy loss at pericenter,

$$\Delta E_p = \varepsilon \frac{Gm^2}{\mathcal{R}} \left(\frac{\mathcal{R}}{r_p} \right)^\beta, \quad (32)$$

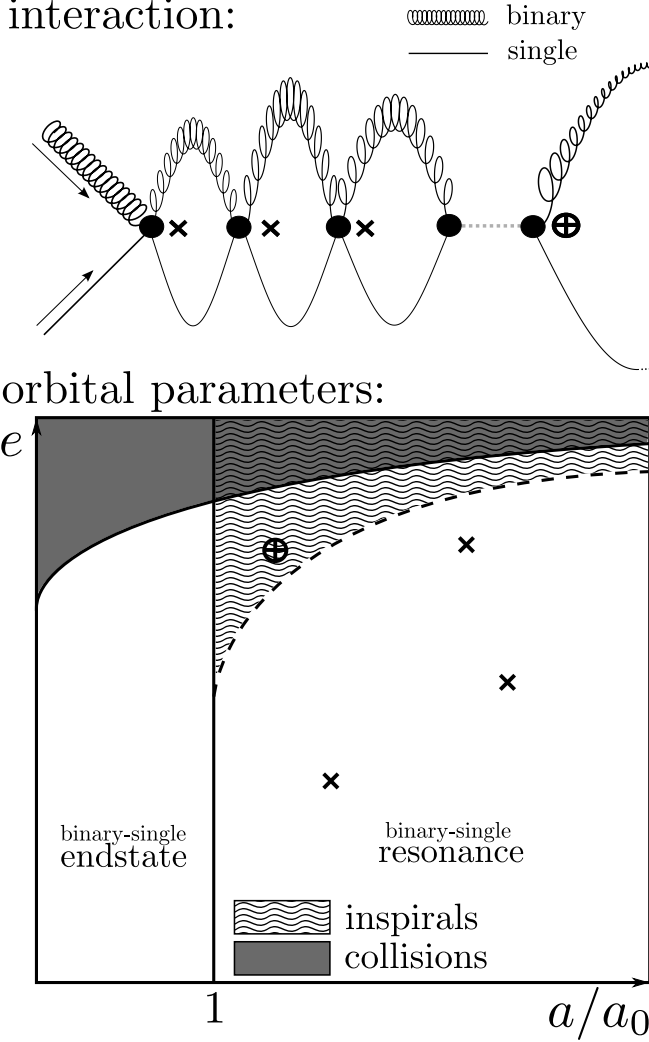


FIG. 5.— Illustration of a resonant binary-single interaction in real space (top) and orbital phase space (bottom), with regions highlighting where inspirals and collisions can form. *Top*: Illustration of a resonant binary-single interaction evolving towards its endstate, which is here an inspiral, from left to right. As illustrated, a resonant system often evolves through a series of intermediate binary-single states characterized by an IMS binary with a bound single. Each time all three objects come together (large black dots), the objects mix and each IMS binary can therefore consist of any two of the three objects. A general evolution can consist of many such intermediate binary-single states, which are here denoted by a series of small grey dots. The IMS binaries are formed with a wide distribution in semimajor axis a and eccentricity e . If the corresponding pericenter distance is small enough, GW radiation or tidal effects will lead to a significant orbital energy loss at pericenter. As a result, the IMS binary will quickly spiral in with a possible merger to follow – similar to GW or tidal captures in the field. *Bottom*: Orbital phase space spanned by a/a_0 , where a_0 is the initial semimajor axis, and e is the eccentricity. Each IMS binary is formed somewhere in this space (a few examples which match with the illustration at the top are shown by the small thick symbols) with a non-negligible probability for either be formed in the inspiral region (wavy part) or collision region (solid grey). The areas of the two regions scale differently with a_0 , which makes collisions dominant at low a_0 and inspirals at high a_0 (see Section 6.2). If a binary is formed to the left of $a/a_0 = 1$, a classical binary-unbound-single endstate has been formed, such as an exchange. Section 5 explains this in detail.

where \mathcal{E} is a normalization factor, and \mathcal{R} is a characteristic radius. This form represents GR and tidal effects reasonably well, as now will be described.

5.2.1. Energy Losses from Gravitational Waves

For GR the leading order dissipative term is quadrupole GW radiation (Peters 1964), which in the high eccentric equal

mass case leads to the following orbital energy loss at each pericenter passage (Hansen 1972),

$$\Delta E_{\text{GW}} \approx \frac{85\pi}{12} \frac{G^{7/2}}{c^5} \frac{m^{9/2}}{r_p^{7/2}}. \quad (33)$$

By a simple rearrangement one finds the above formulation for ΔE_{GW} can be expressed equally by Equation (32), by setting

$$\beta = \frac{7}{2}, \quad \mathcal{E} = \frac{85\pi\sqrt{2}}{96}, \quad \mathcal{R} = R_s = \frac{2Gm}{c^2}, \quad (34)$$

where R_s is here the Schwarzschild radius of an object with mass m .

5.2.2. Energy Losses from Stellar Tides

For tides, the energy deposited into tidal mode oscillations during a single pericenter passage is to leading order ($l = 2$ quadrupole tides) in the PT formalism given by,

$$\Delta E_{\text{tid}} \approx \frac{Gm^2}{R} \left(\frac{R}{r_p}\right)^6 T_2(\eta), \quad (35)$$

where R is the stellar radius, and $T_2(\eta)$ is a non-trivial function which depends on the stellar structure and the dimensionless parameter η , which in the equal mass case equals

$$\eta = \frac{1}{\sqrt{2}} \left(\frac{R}{r_p}\right)^{-3/2}. \quad (36)$$

For our analytical model we approximate $T_2(\eta)$ by a simple powerlaw of the form,

$$T_2(\eta) \approx A\eta^{-\alpha}. \quad (37)$$

This approximation was also used in, e.g., McMillan (1986) and Lai et al. (1993a). From combining the terms we see that in the case of tides, the form for ΔE_{tid} can be expressed by Equation (32) with

$$\beta = 6 + \frac{3\alpha}{2}, \quad \mathcal{E} = A\sqrt{2}^\alpha, \quad \mathcal{R} = R. \quad (38)$$

For our analytical estimations in this work we use $\beta = 9$ ($\alpha = 2$), which is applicable for the $n = 3$ polytropic examples we study here.

5.2.3. Resultant Inspiral Time

With the general form for ΔE_p given by Equation (32), one can now write the inspiral time t_{insp} from Equation (28) as,

$$t_{\text{insp}} = 2\pi r_p^\beta \sqrt{a} \frac{\mathcal{R}^{1-\beta}}{\mathcal{E}\sqrt{2m}}. \quad (39)$$

In the following section we compare this time with the isolation time to find which IMS binaries that are able to undergo an inspiral.

5.3. Formation of Inspirals in Orbital Phase Space

An IMS binary is able to undergo an inspiral if its inspiral time is less than the isolation time. The set of IMS binaries that are able to inspiral can therefore be found by first finding the combination of a' and e which fulfills $t_{\text{insp}} = t_{\text{iso}}$. In this case we find the following relation,

$$\epsilon_{\text{insp}} = \mathcal{E}^{1/\beta} (a_0/\mathcal{R})^{1/\beta-1} \left[\frac{4}{\sqrt{3}} \frac{a'}{a'^\beta (a'-1)^{3/2}} \right]^{1/\beta}, \quad (40)$$

where $\epsilon_{\text{insp}} \equiv 1 - e_{\text{insp}}$, and e_{insp} is the eccentricity. This formula relates the semimajor axis, a' , of an IMS binary to the eccentricity, e_{insp} , the binary must have to exactly spiral in before the single returns. If the eccentricity is larger than e_{insp} (closer to 1), the pericenter is smaller, which results in a faster inspiral due to the increased energy loss at pericenter. Equation (40) therefore defines the boundary of the region in orbital phase space (spanned by a, e) in which inspirals can form ($\epsilon < \epsilon_{\text{insp}}$). This is shown in Figure 5 and further explained in the corresponding caption.

5.4. Inspirational Cross Section

The cross section for an outcome x arising from a RI, can be factorized in the following way (Samsing et al. 2014),

$$\sigma_x = \sigma_{\text{RI}} \times P(x|\text{RI}), \quad (41)$$

where σ_{RI} is the cross section for a binary-single interaction to evolve as a RI, and $P(x|\text{RI})$ is the probability for x to be an endstate given the interaction is a RI. To estimate the inspiral cross section we must therefore calculate the probability for an inspiral to form during a resonant interaction, $P(\text{insp}|\text{RI})$. This term is proportional to the probability for an IMS binary to form with parameters a', e inside the inspiral region (see Section 5.3 above) doing a resonance. In Samsing et al. (2014) it was shown that the distribution in a' and e sampled in a resonance is approximately flat at high eccentricity, as a result, the relative probability for a binary to form in some high eccentricity region scales with the area of that region. The majority of inspirals have a very high eccentricity (Samsing et al. 2014), therefore the probability for forming an inspiral is proportional to the area of the inspiral region. This area is found by integrating ϵ_{insp} from Equation (40) over a' from $a' \approx 1$ to $a' \approx 2$ (when $a' \gtrsim 2$ the triple system can no longer be considered as a binary with a bound single). The a' dependent term in the brackets from Equation (40) integrates to a constant, so the area, and thereby the inspiral probability, will simply scale as,

$$P(\text{insp}|\text{RI}) \propto \mathcal{E}^{1/\beta} (a_0/\mathcal{R})^{1/\beta-1}. \quad (42)$$

As a result, the inspiral probability, has dependence only on the strength of the loss term \mathcal{E} , its slope β , and the compactness of the initial binary (a_0/\mathcal{R}). In the HB limit σ_{RI} is proportional to the CI cross section σ_{CI} from Equation (1). Writing out Equation (41) for inspirals we now finally find the inspiral cross section to scale as,

$$\sigma_{\text{insp}} \propto \frac{m\mathcal{R}}{v_\infty^2} \left[\mathcal{E}^{1/\beta} \left(\frac{a_0}{\mathcal{R}} \right)^{1/\beta} \right] \quad (43)$$

From this relation we can conclude that the cross section for any kind of inspiral *always increases* with a_0 (since β is always positive). The rate of inspirals resulting from any pericenter-dependent loss term is therefore dominated by widely separated binaries and not tight binaries, as one might naively guess. This was illustrated for GW inspirals in Samsing et al. (2014), however, here we have generalized the framework to show that this actually is a generic feature of any kind of inspiral, including tidal inspirals.

5.5. Collision Cross Section

The collision cross section, σ_{coll} , can be estimated by a similar approach as the one described for inspirals. As described in Section 3.2.3, we define a collision to be when two objects

pass each other at a distance smaller than their total unperturbed radii without inspiraling first. In the case of an IMS binary composed of a point-mass perturber and a tidal object with radius R , a collision will therefore occur if the pericenter distance, r_p , is smaller than R . To estimate the cross section for such a collision we first need to calculate the minimum eccentricity, e_{coll} , a temporary formed binary with semimajor axis a' must have to collide. For this we use the standard relation $r_p = a_0 a' (1 - e)$ and substitute r_p with R , from which we now find,

$$\epsilon_{\text{coll}} = \frac{R}{a_0 a'}, \quad (44)$$

where $\epsilon_{\text{coll}} \equiv 1 - e_{\text{coll}}$. This relation defines the boundary of the collision region in orbital phase space illustrated in Figure 5. As for the inspirals, integrating ϵ_{coll} over a' lead us to the relevant scaling for the collision probability given a RI,

$$P(\text{coll}|\text{RI}) \propto R/a_0. \quad (45)$$

This can now be converted into a cross section using Equation (41),

$$\sigma_{\text{coll}} \propto \frac{mR}{v_\infty^2}. \quad (46)$$

The collision cross section is therefore independent of a_0 and linear in R .

By comparing our analytical expressions for the tidal inspiral cross section (in which case \mathcal{R} should be replaced by R) and the collision cross section we observe a few interesting similarities. First, we see that the tidal inspiral cross section approaches the collision cross section as $\beta \rightarrow \infty$. In terms of cross sections, our simple β -model from Equation (32) therefore seems to be the appropriate leading order extension for describing effects related to finite sizes, including non-dissipative solid-sphere collisions. Second, we notice that the inspiral cross section is similar to the collision cross section if the star is treated as a solid sphere with radius $\propto R(a_0/R)^{1/\beta}$ instead of just R . The relevant radius of the star is therefore not just a constant times its radius – it further includes a factor that scales with the energy of the few-body system it evolves in. This was also noticed by our simple scalings in Section 2.3.

5.6. Inspirals in the Collision Dominated Regime

The inspiral and collision regions in orbit space overlap as illustrated in Figure 5, which means that IMS binaries with high enough eccentricity will collide instead of spiraling in. We did not take this into account when calculating the inspiral cross sections in Section 5.4. With the understanding of where collisions form from Section 5.5, we can now correct for this overlap. We only write out the solution for tidal inspirals, since the correction is never really important for GW inspirals – we therefore replace \mathcal{R} with R below.

The asymptotic inspiral solution given by Equation (43) assumed that inspirals can form in the full inspiral area, we can therefore write the collision corrected solution, here denoted by $\sigma_{\text{insp-c}}$, as a product of the asymptotic solution where collisions play no role, σ_{insp} , and a weight term specifying the fraction of the full inspiral area that is not overlapping with the collision area. In Figure 5 this is the wavy region between the dashed and the solid line. The collision corrected inspiral cross section can therefore be written as,

$$\sigma_{\text{insp-c}} \approx \sigma_{\text{insp}} \left[\frac{\int_1^{a'_{\text{ic}}} (\epsilon_{\text{insp}} - \epsilon_{\text{coll}}) da'}{\int_1^{a'_0} \epsilon_{\text{insp}} da'} \right], \quad (47)$$

where a'_{ic} is where ϵ_{insp} crosses ϵ_{coll} , and a'_u is the maximum value for a' ($a'_u \approx 2$). Assuming we know the normalizations of σ_{coll} and σ_{insp} , one can now solve for the full collision corrected inspiral cross section, $\sigma_{\text{insp-c}}$. This will be done using numerical techniques in the next section. However, even without normalizations, we can estimate how $\sigma_{\text{insp-c}}$ scales with a_0/R in the limit where collisions dominate. In this regime we know that a'_{ic} must be close to 1 in which case a'_{ic} to leading order can be written as,

$$a'_{ic} \approx 1 + \left(\frac{4\mathcal{E} a_0}{\sqrt{3} R} \right)^{2/3}. \quad (48)$$

In this limit the integrals in Equation (47) can also be solved by Taylor expanding around $\delta = 0$, where we here define for convenience $\delta \equiv a'_{ic} - 1$. As a result, the $a'^{1/\beta-1}$ term in ϵ_{insp} can be dropped which leaves us with the term $(a' - 1)^{-3/(2\beta)}$ and ϵ_{insp} can now be trivially integrated. The integral over ϵ_{coll} is also easily found and will scale $\propto \ln(1+\delta)$, which is $\approx \delta$ when $\delta \ll 1$. By writing out the full expression in Equation (47) following these assumptions, we find the scaling $\sigma_{\text{insp-c}} \propto a_0^{2/3}$, which holds in the low a_0/R limit.

To summarize, the inspiral cross section scales differently with a_0 depending on if collisions are dominating ($a_0/R \rightarrow 1$) or not ($a_0/R \rightarrow \infty$), with specific scaling solutions given by,

$$\sigma_{\text{insp-c}} \propto a_0^{1/\beta}, \quad (a_0/R) \rightarrow \infty \quad (49)$$

$$\sigma_{\text{insp-c}} \propto a_0^{2/3}, \quad (a_0/R) \rightarrow 1. \quad (50)$$

Cross section results from a full integration of Equation (47) including correct normalizations are shown in Figure 6, and will be discussed in the following section.

5.7. Numerical Calibration of Analytical Cross Sections

We here show the analytical cross sections with correct normalizations estimated using our numerical simulations from Section 4 with tides and GR. As for the analytical results, the scalings presented in this section are only valid in the equal mass case. The cross sections are given in the following rescaled form for convenience,

$$\bar{\sigma} \equiv \sigma \left[\frac{(m/M_\odot)(\mathcal{R}/R_\odot)}{(v_\infty/\text{km s}^{-1})^2} \right]^{-1}. \quad (51)$$

Since the collision corrected tidal inspiral cross section from Section 5.6 has no closed form across the full interval in a_0/R , we instead present tidal inspirals plus collisions which, in our model, scales as $(a_0/R)^{1/9}$ for $\log(a_0/R) > 1$ (see Figure 6).

5.7.1. Cross Sections

The analytical cross section for a tidal extended object and a point-mass perturber to undergo a tidal inspiral *or* a collision (the total coalescence rate) is given by,

$$\bar{\sigma}_{\text{insp,tid}} + \bar{\sigma}_{\text{coll}} \approx 727 \left(\frac{a_0}{R} \right)^{1/9} \text{AU}^2, \quad (52)$$

for $\log(a_0/R) > 1$. The normalization is here valid for polytropes with index $n = 3$ (the exact value for γ do not play a significant role here). The cross section for two compact objects to undergo a GW inspiral is,

$$\bar{\sigma}_{\text{insp,GW}} \approx 2095 \left(\frac{a_0}{R_s} \right)^{2/7} \text{AU}^2. \quad (53)$$

A compact object is here either a NS or a BH – a WD is not compact enough for GWs to dominate over tides during close encounters. For a collision between an extended tidal object and a point-mass perturber we find,

$$\bar{\sigma}_{\text{coll}} \approx 924 \text{AU}^2. \quad (54)$$

A few examples are given below.

5.7.2. Examples

To illustrate how to use the scaling relations from above, let us now consider three examples related to the binary-single interaction between a NS($1.2M_\odot$) and a [WD($1.2M_\odot$, $0.006R_\odot$)-NS($1.2M_\odot$)] binary with $a_0 = 5\text{AU} \approx 1075R_\odot$ in a cluster with $v_\infty = 10 \text{km s}^{-1}$.

- *Tidal inspirals + collisions:* The total WD-NS coalescence cross section (tidal inspirals + collisions) can be estimated using Equation (52) from which we find $\sigma_{\text{insp,tid}} + \sigma_{\text{coll}} \approx 2 \cdot [1.2 \cdot 0.006/10^2] \cdot 727 \cdot (1075.0/0.006)^{1/9} \text{AU}^2 \approx 0.4 \text{AU}^2$. The factor 2 in front accounts for the two WD-NS combinations due to the two NSs in the system.
- *GW inspirals:* The NS-NS GW inspiral cross section is found to be $\sigma_{\text{insp,GW}} \approx 1 \cdot [1.2 \cdot (5.1 \cdot 10^{-6})/10^2] \cdot 2095 \cdot (1075.0/5.1 \cdot 10^{-6})^{2/7} \text{AU}^2 \approx 0.03 \text{AU}^2$, by using Equation (53).
- *Collisions:* The WD-NS collision cross section is found from Equation (54) to be $\sigma_{\text{coll}} \approx 2 \cdot [1.2 \cdot 0.006/10^2] \cdot 924 \text{AU}^2 \approx 0.1 \text{AU}^2$.

In this particular example we see that the inclusion of tides results in a total WD-NS coalescence cross section that is about four times higher than the one estimated from the simple sticky star collision criterion. One can compare these estimates with the upper left plot in Figure 4. In an upcoming paper we extend this analytical framework to systems where the WD can have any mass.

5.7.3. Summary: Analytical Estimation of Cross Sections

The calibrated cross sections from the section above including collision corrected tidal inspirals are plotted and discussed in Figure 6. The tidal and GW inspiral cross sections are also shown in Figure 4 with dashed and dashed-dotted lines, respectively. We see that our derived scalings do indeed work all the way from a WD to a MS star across almost four orders of magnitudes in a_0 . Our analytical predictions give valuable insight into how the collisions and inspirals possibly scale around the HB limit.

6. DISCUSSION

Our main findings, their consequences and relative importance in different dynamical systems are discussed below.

6.1. Stellar Collision Rate Not Enhanced By Tides

Our initial motivation for this study was to explore if the modified dynamics arising from tidal modes coupling to the orbital motion can enhance mergers or collisions in chaotic binary-single interactions. Using full numerical simulations and analytical arguments, we have learned that the most significant change when including tides is the formation of tidal inspirals – similar to tidal captures in the field.

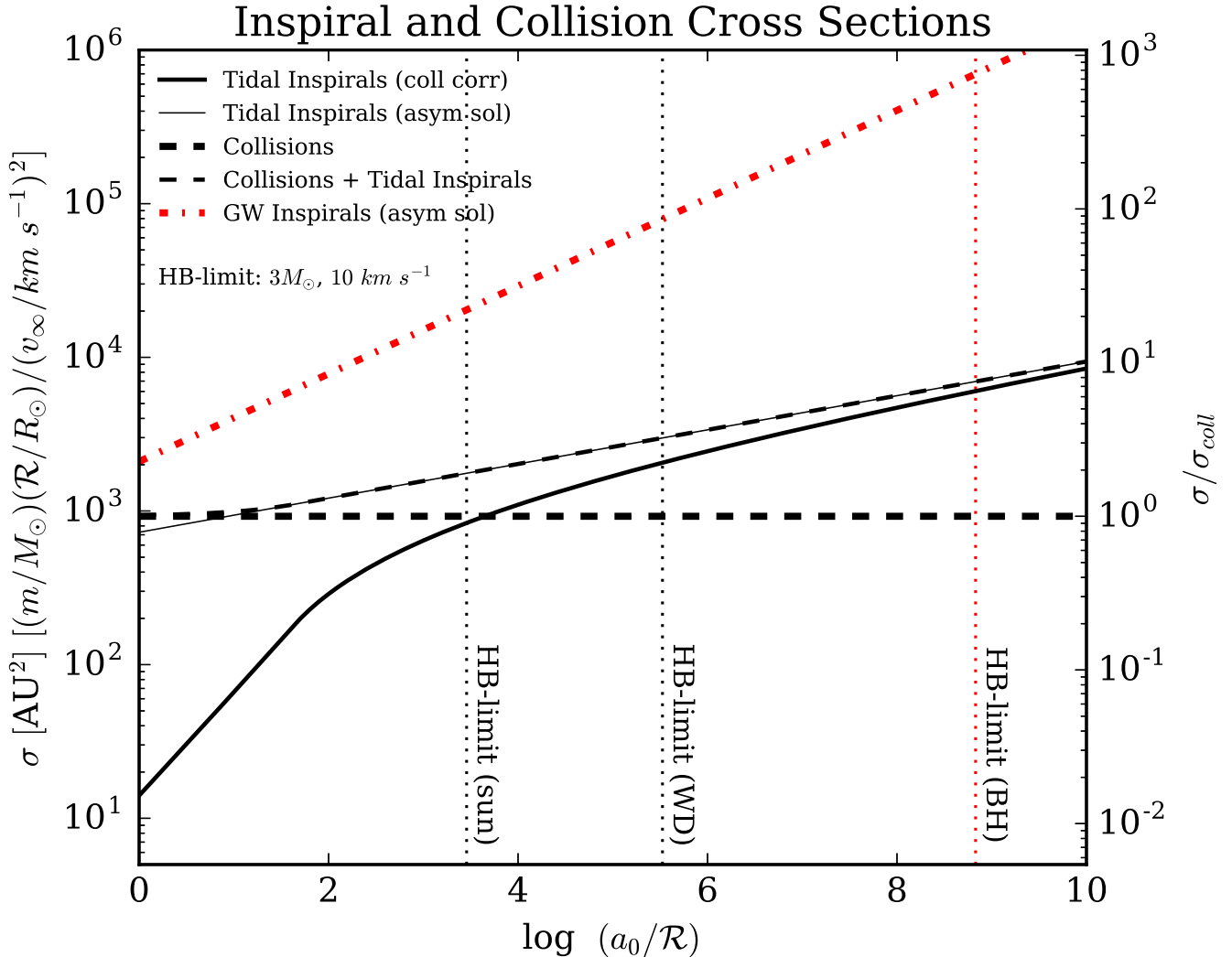


FIG. 6.— Summary of outcome cross sections σ related to finite size effects (collisions), tidal effects (tidal inspirals) and GR effects (GW inspirals) arising from equal mass binary-single interactions. The black lines show the cross sections for an extended tidal object and a point-mass perturber to either undergo a tidal inspiral (thick black solid line) or a sticky star collision (thick horizontal dashed line). The thin black line illustrates the analytical asymptotic solution to the tidal inspiral cross section where the thin dashed line shows the collision + tidal inspiral cross section. The thick black line deviates from the asymptotic solution due to the overlap between collisions and tidal inspirals in orbital phase space at especially small a_0/R (see discussion in Section 5.6). The tidal inspiral cross section shown here is valid for $n = 3$ polytropes. The red dash-dotted line shows the cross section for two compact objects (NS or BH) to undergo a GW inspiral. The left y-axis shows σ in units of $[(m/M_\odot)(\mathcal{R}/R_\odot)/(v_\infty/\text{km s}^{-1})^2]$, where v_∞ is the velocity dispersion, m is the mass of one of the (equal mass) interacting objects, and \mathcal{R} is the corresponding radius, which for tidal inspirals and collisions is the physical radius and for GW inspirals is the Schwarzschild radius. A few examples are given in Section 5.7. The right y-axis shows σ in units of σ_{coll} . The functional form of the cross sections are based on our analytical framework from Section 5, where the normalizations are estimated using our simulations with tides and GR from Section 4. The three vertical dotted lines show from left to right a_{HB}/R for a system with $v_\infty = 10 \text{ km s}^{-1}$ and $m = 1M_\odot$ (corresponding to $a_{\text{HB}} \approx 13.3\text{AU}$), when $R = 1R_\odot$ (solar type star), $R = 0.0086R_\odot$ (WD) and $R = 4.24 \cdot 10^{-6}$ (BH Schwarzschild radius), respectively. The corresponding cross sections are only valid to the left of these lines. At this velocity dispersion, tidal inspirals with a solar type star can not dominate the coalescence rate within the hard HB limit, but if the tidal object is a WD then tides can actually lead to an enhanced coalescence rate by about a factor of four. The cross sections from this plot are overplotted our simulation data in Figure 4.

The main reason why the collision or merger rate is not drastically altered by tides is that this would require the resonant system to undergo (at least) two independent close passages; one that first drains some of the orbital energy through tides without leading to an inspiral, and then one that results in the actual merger. However, mergers – and thereby close passages – are relatively rare, therefore the rate of collisions following a previous close passage will happen only rarely. If the collision probability is P_{coll} then the tidally induced collision probability will be of order $\approx P_{\text{coll}}^2$. For example, in the WD case from Section 4.1.1, $P_{\text{coll}} \approx 10^{-3}$ at $a_0 = 1\text{AU}$. In fact, tides tend instead to decrease the number of collisions

because a system that could have evolved into a collision now can end as an inspiral. This is only seen at very low a_0 .

We initially speculated that if tides could turn a fraction of the DIs into RIs (the encounter could be tidally captured into the triple system), the collision probability will be enhanced. However, the effective cross section for this to happen is simply too small. If it did happen, the maximum enhancement would still only be about a factor of two since the ratio between the number of DIs and RIs initially is about unity in the equal mass case (Samsing et al. 2014). A barrier for forming actual mergers is also the angular momentum, L . Even our inspirals, which represent the highest energy and momentum loss configurations in our simulations, do not collide due

to the requirement of L to be (almost) conserved (see Section 3.2.1). For a more accurate description one must include mass loss and dissipation, which requires the use of hydrodynamical simulations (Gaburov et al. 2010). Further discussion on the collision rates in general N-body systems can be found in Leigh & Geller (2012, 2015).

6.2. Tidal Inspirals and Collisions in Cluster Systems

Studies indicate that tidal captures are more likely to merge than to form a stable binary; see e.g. discussion in Rasio (1993). A key question is then at what fraction our 3-body tidal inspiral mergers contribute to the stellar coalescence rate compared to the classical sticky star collisions. We can use our analytical framework to gain some insight into this question by considering the ratio between the tidal inspiral and collision cross sections given by Equations (43) and (46), respectively,

$$\frac{\sigma_{\text{insp}}}{\sigma_{\text{coll}}} \propto \left(\frac{a_0}{R}\right)^{1/\beta}. \quad (55)$$

This relation shows that the rate of inspirals relative to collisions increases as the size of the interacting objects decreases and as a_0 increases. The maximum value of $\sigma_{\text{insp}}/\sigma_{\text{coll}}$ for an object with radius R , is set by the hard binary limit $a_{\text{HB}} \propto m/v_\infty^2$ (see Equation 3), from which we derive

$$\max\left(\frac{\sigma_{\text{insp}}}{\sigma_{\text{coll}}}\right) \propto \left(\frac{1}{v_\infty^2} \frac{m}{R}\right)^{1/\beta} \propto \left(\frac{v_{\text{esc}}}{v_\infty}\right)^{2/\beta}, \quad (56)$$

where v_{esc} is the escape velocity of the tidal object. From the equation above we can conclude that the more compact the interacting objects are (i.e., the larger m/R is), the more inspirals can form relative to collisions. This is also seen in our simulation results described in Section 4, and in Figure 6.

The compactness m/R required for an object to produce tidal inspirals with a point-mass perturber at the same rate as collisions, can be read off Figure 6. This figure shows that the tidal inspiral rate is similar to the collision rate when $\log(a_0/R) \approx 3.5$. If we use the hard binary value a_{HB} from Equation (3), we find

$$\frac{m/M_\odot}{R/R_\odot} \approx 10^{-2} \left(\frac{v_\infty}{\text{km s}^{-1}}\right)^2 \text{ when } \sigma_{\text{coll}} \approx \sigma_{\text{insp}}(a_{\text{HB}}). \quad (57)$$

This gives the critical value of m/R in the HB limit. That is, if the tidal object has an m/R larger than this value then tidal inspirals can dominate over collisions. Figure 7 shows the relation from Equation (57) for different values of v_∞ , together with some simplified mass-radius relations for MS ($R \propto M^{0.8}$ – dashed line) and WDs (see Zalamea et al. (2010) – solid line). We see that if the tidal object is a WD, tidal inspirals can be as important as collisions in GC systems ($v_\infty = 10 \text{ km s}^{-1}$) and might even also play a role in galactic nuclei ($v_\infty = 100 \text{ km s}^{-1}$). If the tidal object is a MS star, the rate of inspirals is much lower compared to the rate of collisions, and inspirals will only contribute to the coalescence rate in clusters with a $\approx 1 \text{ km s}^{-1}$ dispersion. Interestingly enough, low dispersion clusters do have a high fraction of wide binaries and are also surprisingly dynamically active (see discussion in e.g. Leigh & Geller 2013). Again, to make this picture applicable for describing more realistic astrophysical scenarios we need to carefully work out the unequal mass case.

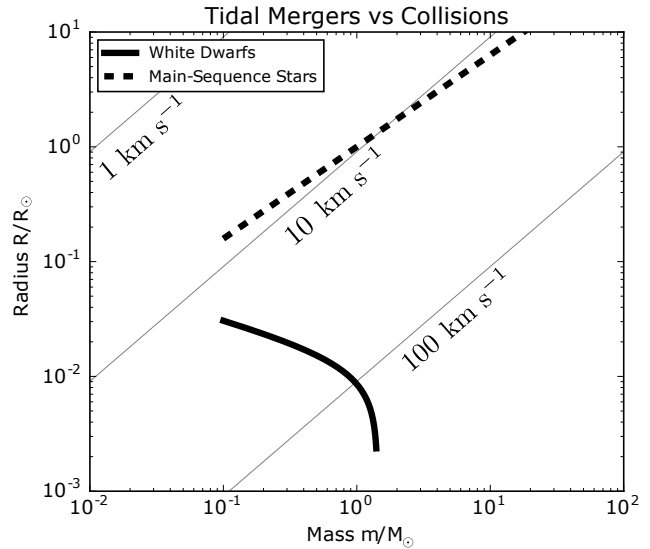


FIG. 7.— Relation between compactness m/R , velocity dispersion v_∞ , and the rate of tidal inspirals relative to collisions. The thin solid grey lines show the combinations of m , R and v_∞ from Equation (57) that will result in an equal number of tidal inspirals and collisions in the HB limit ($a_0 = a_{\text{HB}}$). We assume the equal mass case and the tidal inspirals are here between an extended tidal object and a point-mass perturber. Also shown are simplified mass-radius relationships for white dwarfs (solid line) and main sequence stars (dashed line). If a given combination of m and R is to the right of a grey line, tidal inspirals will dominate over collisions in the HB limit for the corresponding v_∞ . We see that WDs are the only objects compact enough to produce a significant number of tidal inspirals relative to collisions in a typical GC (10 km s^{-1}), where MS star tidal inspirals probably only contribute to the coalescence rate in open clusters (1 km s^{-1}).

6.3. GW and Electromagnetic Signatures from Tidal Inspirals

Tidal and GW inspirals are characterized by high eccentricity and low angular momentum (Figure 8). The high eccentricity especially allows for multiple close passages before merger which will give rise to unique electromagnetic (EM) and GW observables, especially when the tidal object is a WD (Paschalidis et al. 2009, 2011a,b). The GW signal will have a very rich spectrum compared to normal circular inspirals (Willems et al. 2007; Lorén-Aguilar et al. 2010), which will reveal much more information about especially the equation of state of the WD.

As seen in Figure 8, a space-borne GW instrument like LISA will be sensitive to these WD-NS inspirals. However, while there are plenty of interesting physics in high eccentricity WD-NS tidal inspirals and collisions, the rates are expected to be modest from the binary-single channel: if we consider the $0.6M_\odot$ WD case from Samsing et al. (2014) and assume that the inclusion of tides enhances the resultant merger rate by a factor of 5 (a $0.6M_\odot$ WD both has a lower polytropic index n and an $\alpha \sim 0$, which is expected to lead to more inspirals compared to a heavy WD), then the expected rate of WD-NS tidal inspirals will be around $\approx 50 \text{ yr}^{-1} \text{ Gpc}^{-3}$. The problem here is that the associated GW strain is far too weak for these sources to be seen outside our own galaxy by LISA. More promising signatures could be thermonuclear optical transients (Khokhlov & Ergma 1986; Lee & Ramirez-Ruiz 2007; Raskin et al. 2009; Rosswog et al. 2009; Sim et al. 2010; Perets et al. 2010; Waldman et al. 2011; Raskin et al. 2012; Metzger 2012; Holcomb et al. 2013), and high-energy transients (Fryer & Woosley 1998; Fryer et al. 1999; Lee & Ramirez-Ruiz 2007) that are expected to ensue when both light and heavy WDs are shocked in collisions or merg-

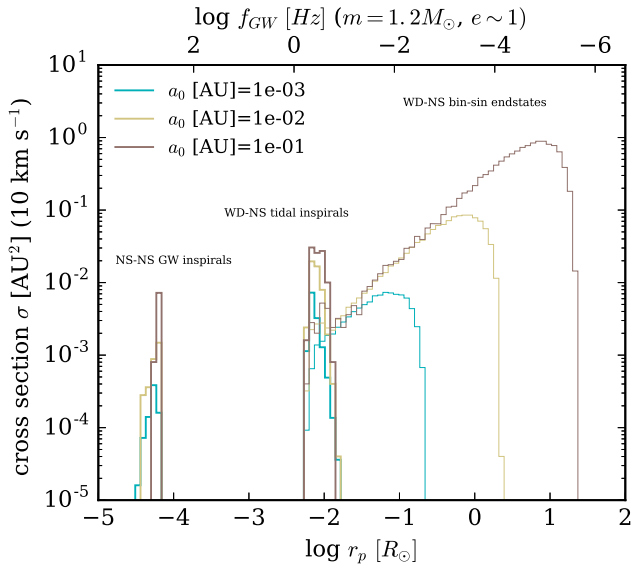


FIG. 8.— Outcome cross section σ , as a function of the pericenter distance r_p of the endstate binary, computed from a set of 5×10^4 binary-single interactions between a $[\text{NS}(1.2M_\odot), \text{WD}(1.2M_\odot)]$ binary and a single incoming $\text{NS}(1.2M_\odot)$. The *thin solid lines* show the distribution of WD-NS binaries from binary-unbound-single endstates (such as an exchange or a fly-by). The *thick solid lines* show the distribution of inspirals, where the left and right peak is the NS-NS GW inspirals and WD-NS tidal inspirals, respectively. These inspiral populations only appear when tides and GR are included in the EOM of the N -body system. Inspirals are characterized by very low angular momentum corresponding to a small pericenter when $e \sim 1$, which makes them interesting sources for both EM and GW signals. From the upper axis showing the corresponding GW frequency f_{GW} , we see that GW inspirals fall within the LIGO sensitivity band, where the tidal inspirals are closer to the LISA band. These results greatly motivates further studies of compact objects undergoing a high eccentricity evolution. The cross section as a function of a_0 is shown for the same set in Figure 4.

ers with COs. The exact rates of such encounters requires a detailed understanding of unequal mass scatterings involving WDs and COs with tides and GR, which we plan to consider in future work.

7. CONCLUSION

We present the first systematic study of how dynamical tides affect the interaction and relative outcomes in binary-single interactions. From performing a large set of binary-single scatterings using an N -body code that includes tides and GR, we find that the inclusion of tides leads to a population of tidal captures which are occurring during the chaotic

evolution of the triple interaction. We denote these captures *tidal inspirals*, partly due to their similarity with the GW inspirals studied in (Samsing et al. 2014).

We confirm with analytical models that the rate of tidal inspirals relative to the classical sticky star collision rate increases with (a_0/R) , as a result, tides show the largest effect for widely separated binaries. Since the upper limit on a_0 is set by the HB limit, which scales linearly with mass m , we conclude that the compactness m/R of the tidal object is the key factor for determining if tides play a significant role or not in a given cluster environment: a larger compactness leads to more tidal inspirals relative to collisions. As a result of these scalings, we find that the only tidal object which is compact enough to have tidal inspirals dominating over collisions in a typical GC environment is a WD.

We further conclude that tides, from a dynamical perspective, do not seem to effect the dense stellar system as a whole, as otherwise speculated in several previous studies (e.g. Fregeau et al. 2004) – although stellar finite sizes do matter through collisions and dynamical kicks (McMillan 1986). However, the inclusion of tides and GWs leads to a rare, but highly interesting population of eccentric binaries. The high eccentricity likely results in unique EM and GW signals. While highly eccentric binaries can be created in single-single captures, it was illustrated in Samsing et al. (2014) that the binary-single channel is likely the dominant formation path. These observations motivate further dynamical studies on few-body interactions involving especially WDs and COs, as well as hydrodynamical studies on the outcome of highly eccentric captures.

While our estimated inspiral rate involving a heavy WD ($1.2M_\odot$) is still modest, we do expect the rate to be significantly higher for lower mass WDs simply because they are more vulnerable to tidal deformations. We are currently working on the analytical prescriptions for unequal mass encounters.

It is a pleasure to thank D. Spergel, R. Cen, V. Paschalidis, C. Holcomb, T. Ilan, and F. Pretorius for helpful discussions. Support for this work was provided by the David and Lucile Packard Foundation, UCMEXUS (CN-12-578) and NASA through an Einstein Postdoctoral Fellowship grant number PF4-150127, awarded by the Chandra X-ray Center, which is operated by the Smithsonian Astrophysical Observatory for NASA under contract NAS8-03060.

REFERENCES

- Baumgardt, H., Hut, P., & Heggie, D. C. 2002, MNRAS, 336, 1069
 Blanchet, L. 2006, Living Reviews in Relativity, 9
 Camilo, F., & Rasio, F. A. 2005, in Astronomical Society of the Pacific Conference Series, Vol. 328, Binary Radio Pulsars, ed. F. A. Rasio & I. H. Stairs, 147
 Carter, B., & Luminet, J. P. 1985, MNRAS, 212, 23
 Clark, G. W. 1975, ApJ, 199, L143
 Diener, P., Kosovichev, A. G., Kotok, E. V., Novikov, I. D., & Pethick, C. J. 1995, MNRAS, 275, 498
 East, W., Pretorius, F., & Stephens, B. 2012, Phys. Rev. D, 85, 124009
 East, W. E., McWilliams, S. T., Levin, J., & Pretorius, F. 2013, Phys. Rev. D, 87, 043004
 East, W. E., & Pretorius, F. 2012, ApJ, 760, L4
 Fabian, A. C., Pringle, J. E., & Rees, M. J. 1975, MNRAS, 172, 15p
 Fregeau, J. M., Cheung, P., Portegies Zwart, S. F., & Rasio, F. A. 2004, MNRAS, 352, 1
 Fregeau, J. M., Ivanova, N., & Rasio, F. A. 2009, ApJ, 707, 1533
 Freire, P. C. C. 2013, in IAU Symposium, Vol. 291, Neutron Stars and Pulsars: Challenges and Opportunities after 80 years, ed. J. van Leeuwen, 243–250
 Fryer, C. L., & Woosley, S. E. 1998, ApJ, 502, L9
 Fryer, C. L., Woosley, S. E., Herant, M., & Davies, M. B. 1999, ApJ, 520, 650
 Gaburov, E., Lombardi, Jr., J. C., & Portegies Zwart, S. 2010, MNRAS, 402, 105
 Geller, A. M., & Mathieu, R. D. 2011, Nature, 478, 356
 Gold, R., Bernuzzi, S., Thierfelder, M., Brüggmann, B., & Pretorius, F. 2012, Phys. Rev. D, 86, 121501
 Grindlay, J., Zwart, S. P., & McMillan, S. 2006, Nat Phys, 2, 116
 Gültekin, K., Miller, M. C., & Hamilton, D. P. 2006, ApJ, 640, 156
 Hansen, R. 1972, Phys. Rev. D, 5, 1021
 Heggie, D. C. 1975, MNRAS, 173, 729
 Heggie, D. C., & Hut, P. 1993, ApJS, 85, 347

- Holcomb, C., Guillochon, J., De Colle, F., & Ramirez-Ruiz, E. 2013, *ApJ*, 771, 14
- Hut, P. 1983, *ApJ*, 268, 342
- 1993, *ApJ*, 403, 256
- Hut, P., & Bahcall, J. N. 1983, *ApJ*, 268, 319
- Hut, P., & Inagaki, S. 1985, *ApJ*, 298, 502
- Hut, P., & Verbunt, F. 1983, *Nature*, 301, 587
- Hut, P., et al. 1992, *Astronomical Society of the Pacific*, 104, 981
- Ivanov, P. B., Chernyakova, M. A., & Novikov, I. D. 2003, *MNRAS*, 338, 147
- Ivanov, P. B., & Novikov, I. D. 2001, *ApJ*, 549, 467
- Ivanova, N. 2013
- Ivanova, N., Belczynski, K., Fregeau, J. M., & Rasio, F. A. 2005a, *MNRAS*, 358, 572
- Ivanova, N., Chaichenets, S., Fregeau, J., Heinke, C. O., Lombardi, J. C. J., & Woods, T. E. 2010, *ApJ*, 717, 948
- Ivanova, N., Fregeau, J. M., & Rasio, F. A. 2005b, *Binary Radio Pulsars*, 328, 231
- Ivanova, N., Heinke, C. O., Rasio, F. A., Belczynski, K., & Fregeau, J. M. 2008, *MNRAS*, 386, 553
- Ivanova, N., Heinke, C. O., Rasio, F. A., Taam, R. E., Belczynski, K., & Fregeau, J. 2006, *MNRAS*, 372, 1043
- Khokhlov, A. M., & Ergma, E. V. 1986, *Soviet Astronomy Letters*, 12, 152
- Knigge, C. 2015, *Blue Stragglers in Globular Clusters: Observations, Statistics and Physics*, ed. H. M. J. Boffin, G. Carraro, & G. Beccari, 295
- Kochanek, C. S. 1992, *ApJ*, 385, 604
- Kosovichev, A. G., & Novikov, I. D. 1992, *MNRAS*, 258, 715
- Krolik, J. H. 1983, *Nature*, 305, 506
- Kumar, P., & Goodman, J. 1996, *ApJ*, 466, 946
- Lai, D., Rasio, F. A., & Shapiro, S. L. 1993a, *ApJ*, 412, 593
- 1993b, *ApJS*, 88, 205
- 1993c, *ApJ*, 406, L63
- 1994a, *ApJ*, 423, 344
- 1994b, *ApJ*, 420, 811
- 1994c, *ApJ*, 437, 742
- Lai, D., & Shapiro, S. L. 1995, *ApJ*, 443, 705
- Lee, H. M., & Ostriker, J. P. 1986, *ApJ*, 310, 176
- Lee, W. H., & Ramirez-Ruiz, E. 2007, *New J. Phys.*, 9, 17
- Lee, W. H., Ramirez-Ruiz, E., & van de Ven, G. 2010, *ApJ*, 720, 953
- Leigh, N., & Geller, A. M. 2012, *MNRAS*, 425, 2369
- Leigh, N., Knigge, C., Sills, A., Perets, H. B., Sarajedini, A., & Glebbeek, E. 2013, *MNRAS*, 428, 897
- Leigh, N., Sills, A., & Knigge, C. 2011, *MNRAS*, 416, 1410
- Leigh, N. W. C., & Geller, A. M. 2013, *MNRAS*, 432, 2474
- 2015, *MNRAS*, 450, 1724
- Lorén-Aguilar, P., Isern, J., & García-Berro, E. 2010, *MNRAS*, 406, 2749
- Luminet, J. P., & Carter, B. 1986, *ApJS*, 61, 219
- Mardling, R. A. 1995a, *ApJ*, 450, 722
- 1995b, *ApJ*, 450, 732
- Mardling, R. A., & Aarseth, S. J. 2001, *MNRAS*, 321, 398
- McMillan, S. L. W. 1986, *ApJ*, 306, 552
- 1991, In: *The formation and evolution of star clusters (A93-48676 20-90)*, 13, 324
- McMillan, S. L. W., McDermott, P. N., & Taam, R. E. 1987, *ApJ*, 318, 261
- Metzger, B. D. 2012, *MNRAS*, 419, 827
- Naoz, S., Kocsis, B., Loeb, A., & Yunes, N. 2013, *ApJ*, 773, 187
- Novikov, I. D., Pethick, C. J., & Polnarev, A. G. 1992, *MNRAS*, 255, 276
- Ogawaguchi, W., & Kojima, Y. 1996, *Progress of Theoretical Physics*, 96, 901
- Ogilvie, G. I. 2014, *ARA&A*, 52, 171
- Ostriker, J. P. 1985, in *IAU Symposium, Vol. 113, Dynamics of Star Clusters*, ed. J. Goodman & P. Hut, 347–357
- Paschalidis, V., Etienne, Z., Liu, Y. T., & Shapiro, S. L. 2011a, *Phys. Rev. D*, 83, 064002
- Paschalidis, V., Liu, Y. T., Etienne, Z., & Shapiro, S. L. 2011b, *Phys. Rev. D*, 84, 104032
- Paschalidis, V., MacLeod, M., Baumgarte, T. W., & Shapiro, S. L. 2009, *Phys. Rev. D*, 80, 024006
- Perets, H. B., & Fabrycky, D. C. 2009, *ApJ*, 697, 1048
- Perets, H. B., et al. 2010, *Nature*, 465, 322
- Peters, P. 1964, *Phys. Rev.*, 136, B1224
- Pooley, D., & Hut, P. 2006, *ApJ*, 646, L143
- Pooley, D., et al. 2003, *ApJ*, 591, L131
- Press, W. H., & Teukolsky, S. A. 1977, *ApJ*, 213, 183
- Rasio, F. A. 1993, *PASP*, 105, 973
- Raskin, C., Scannapieco, E., Fryer, C., Rockefeller, G., & Timmes, F. X. 2012, *ApJ*, 746, 62
- Raskin, C., Timmes, F. X., Scannapieco, E., Diehl, S., & Fryer, C. 2009, *MNRAS*, 399, L156
- Rosswog, S., Kasen, D., Guillochon, J., & Ramirez-Ruiz, E. 2009, *arXiv.org*
- Samsing, J., MacLeod, M., & Ramirez-Ruiz, E. 2014, *ApJ*, 784, 71
- Sandage, A. R. 1953, *AJ*, 58, 61
- Sigurdsson, S., & Phinney, E. S. 1993, *ApJ*, 415, 631
- 1995, *ApJS*, 99, 609
- Sim, S. A., Röpke, F. K., Hillebrandt, W., Kromer, M., Pakmor, R., Fink, M., Ruiter, A. J., & Seitenzahl, I. R. 2010, *ApJ*, 714, L52
- Stephens, B. C., East, W. E., & Pretorius, F. 2011, *ApJ*, 737, L5
- Valtonen, M., & Karttunen, H. 2006, *The Three-Body Problem*
- Verbunt, F., & Freire, P. C. C. 2014, *A&A*, 561, A11
- Waldman, R., Sauer, D., Livne, E., Perets, H., Glasner, A., Mazzali, P., Truran, J. W., & Gal-Yam, A. 2011, *ApJ*, 738, 21
- Willems, B., Kalogera, V., Vecchio, A., Ivanova, N., Rasio, F. A., Fregeau, J. M., & Belczynski, K. 2007, *ApJ*, 665, L59
- Zalamea, I., Menou, K., & Beloborodov, A. M. 2010, *MNRAS*, 409, L25